REPORT DOCUMENTATION PAGE

Public reporting burden for this collection of information is estimated to average 1 hour per response, including the time for reviewing instructions, searching existing data sources, gathering and maintaining the data needed, and completing and reviewing the collection of information. Send comments regarding this burden estimate or any other aspect of this collection of information, including suggestions for reducing this burden, to Washington Headquarters Services, Directorate for Information Operations and Reports, 1215 Jefferson Davis Highway, Suite 1204, Arlington, VA 22202-4302, and to the Office of Management and Budget, Paperwork Reduction Project (0704-0188), Washington, DC 20503.

1. AGENCY USE ONLY (Leave blank)	2. REPORT DATE	3. REPORT TYPE AND DATES COVERED
	31 January 1996	Final Technical Report 03/01/92-02/28/95

4. TITLE AND SUBTITLE

Manipulation of Airfoil Response in an Unsteady Stream

5. FUNDING NUMBERS

G:F49620-92-J-0178

6. AUTHOR(S)

Chih-Ming Ho

7. PERFORMING ORGANIZATION NAME(S) AND ADDRESS(ES)

University of California, Los Angeles
Mechanical, Aerospace & Nuclear Engineering Department
38-137 Engr. IV, Box 159710
Los Angeles, CA 9009-1597

8. PERFORMING ORGANIZATION

AFOSR-TR-96
0145

9. SPONSORING/MONITORING AGENCY NAME(S) AND ADDRESS(ES)

AFOSR/NA
110 Duncan Avenue, Suite B115
Bolling AFB, DC 20332-0001

Dr Len Sakell   2307CS

NA

10. SPONSORING/MONITORING AGENCY REPORT NUMBER

11. SUPPLEMENTARY NOTES

12a. DISTRIBUTION/AVAILABILITY STATEMENT

12b. DISTRIBUTION CODE

19960404 053

13. ABSTRACT (Maximum 200 words)

Experiments were conducted to investigate the mechanism responsible for vortex breakdown over delta wing. By varying the free stream velocity, unsteady vortex breakdown occurs over the wing due to the alteration of the balance between leading-edge vorticity production and convection. This allows the study of vortex breakdown in both the spatial and temporal domain. It was found that parameters such as swirl angle and circulation do not correlate well with breakdown when the flow is unsteady. However, vortex breakdown seemed to follow the positive feedback mechanism proposed by Brown and Lopez. When breakdown occurs, there is a redistribution of vorticity in the vortex subcore, where the vorticity vector changes from an essentially axial direction to a generally tangential direction. Further, the helix angle for the velocity exceeds that of the vorticity globally in the vortex subcore only in the instant just before breakdown. Finally, it was found that through breakdown, global quantities such as circulation and flow rate varies in phase as the upstream vorticity and velocity changes with time. This implies that the breakdown process is essentially an inviscid mechanism.

14. SUBJECT TERMS

unsteady aerodynamics; delta wing; vortex breakdown

15. NUMBER OF PAGES

59

16. PRICE CODE

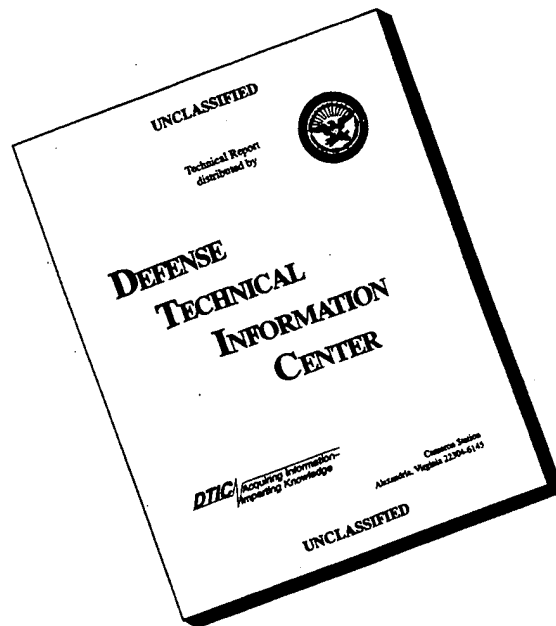| 17. SECURITY CLASSIFICATION OF REPORT	18. SECURITY CLASSIFICATION OF THIS PAGE	19. SECURITY CLASSIFICATION OF ABSTRACT	20. LIMITATION OF ABSTRACT
Unclassified	Unclassified	Unclassified	UL

NSN 7540-01-280-5500

DTIC QUALITY INSPECTED 1

DISCLAIMER NOTICE

UNCLASSIFIED

Technical Report
distributed by

DEFENSE
TECHNICAL
INFORMATION
CENTER

DTIC Acquiring Information-
Imparting Knowledge

Cameron Station
Alexandria, Virginia 22304-6145

UNCLASSIFIED

THIS DOCUMENT IS BEST
QUALITY AVAILABLE. THE
COPY FURNISHED TO DTIC
CONTAINED A SIGNIFICANT
NUMBER OF PAGES WHICH DO
NOT REPRODUCE LEGIBLY.

MANIPULATION OF AIRFOIL RESPONSE IN AN UNSTEADY STREAM

Principal Investigator

Ho, Chih-Ming
Mechanical and Aerospace Engineering Department
University of California, Los Angeles
405 Hilgard Avenue
Los Angeles, CA 90095-1597

Final Technical Report

Contract No. F49620-92-J-0178
March 1, 1992 to February 28, 1995

1. ABSTRACT

Experiments were conducted to investigate the mechanism responsible for vortex breakdown over delta wing. By varying the free stream velocity, unsteady vortex breakdown occurs over the wing due to the alteration of the balance between leading-edge vorticity production and convection. This allows the study of vortex breakdown in both the spatial and temporal domain. It was found that parameters such as swirl angle and circulation do not correlate well with breakdown when the flow is unsteady. However, vortex breakdown seemed to follow the positive feedback mechanism proposed by Brown and Lopez. When breakdown occurs, there is a redistribution of vorticity in the vortex subcore, where the vorticity vector changes from an essentially axial direction to a generally tangential direction. Further, the helix angle for the velocity exceeds that of the vorticity globally in the vortex subcore only in the instant just before breakdown. Finally, it was found that through breakdown, global quantities such as circulation and flow rate varies in phase as the upstream vorticity and velocity changes with time. This implies that the breakdown process is essentially an inviscid mechanism.

2. OBJECTIVE

Since the observation of the breakdown of the leading-edge vortices over a delta wing by Peckham and Atkinson in 1957, the phenomenon of vortex breakdown remains a challenging and unsolved problem in aerodynamics. This problem is especially important for today's high-agility aircraft operating at large angle of attack, since vortex breakdown above the wing results in abrupt change of the aerodynamic characteristics, general unsteadiness, and could lead to loss of control. Despite the many theoretical, experimental, and computational studies in the past, the fundamental mechanism responsible for the breakdown of the leading-edge vortices is not clearly understood. Many of the theoretical models fails to explain the physical mechanism that brings about vortex breakdown. Most of the theories can predict vortex breakdown to occur within the observed range of swirl angles and the sensitivity of breakdown to an axial pressure gradient, but none of the theories can predict the flow in the breakdown region and the location of breakdown with an accuracy sufficient to be checked against experimental measurements. However, if the

1

fundamental mechanism for breakdown can be clarified, the insight could lead to prediction of breakdown position and the development of appropriate control techniques.

The unsteady water channel at UCLA provides an unique experimental apparatus to study vortex breakdown. The water channel can provide highly-controlled large-amplitude velocity variation, thus enables us to study both the temporal and the spatial evolution of the velocity and vorticity field within the breakdown region. Combined with LDA measurements and flow visualization studies, we have investigated various vortex breakdown criteria and have attempted to clarify the underlying physical mechanism behind vortex breakdown.

3. VORTICAL STRUCTURES OVER DELTA WINGS

Vortical structures over delta wings result from boundary layer separation along the leading-edges. The separations generate shear layers that lead to the formation of two primary vortices above the wing. These vortices are important because they produce up to 60% of the total lift at high angle of attack (Wentz and Kohlman 1971).

The flowfield about the leading-edge vortex is nearly axisymmetric around the vortical axis. Contrary to confined vortices generated with guidevane in vortex tubes, vortex generated by a swept delta wing is formed from the roll-up of the vortex sheet which is continuously shed from the leading-edge, so that a significant variation with axial distance along the vortex is an inherent aspect of the vortex structure. The vortex in a tube is highly axisymmetrical, radially confined and normally subject to only slow axial variations. The flowfield over the delta wing can be characterized by its two primary velocity components, the axial component $V_x(r,x)$, and the swirl or azimuthal component $V_\phi(r,x)$. The radial component V_r is always small except when breakdown occurs.

Figure 1 shows the typical flow profile before and after vortex breakdown. When there is no vortex breakdown, the axial velocity has a jet-like profile, with the centerline velocity that is almost twice the freestream value. However, when breakdown occurs, axial velocity changes to a wake-like profile, with a deficit in the centerline velocity. Contrary to axial velocity, which shows significant differences before and after breakdown, the swirl velocity does not deviate

2

much from the norm. In fact, it is difficult to determine when breakdown has occurred from the swirl velocity alone.

The flowfield inside the spiraling vortices can be divided into two main regions: a *viscous subcore* and a *outer inviscid rotational core*. In the outer part of the flow, the vortex motion approximates to irrotational behavior for which the swirl velocity varies as $V_\theta \sim \frac{1}{r}$. On the other hand, near the vortex centerline, viscous effects are important, and the swirl velocity behaves like solid body rotation for which $V_\theta \sim r$ (figure 2, where r_c is the radius of the vortex subcore). For an ideal vortex that is axisymmetric, the swirl velocity profile should be anti-symmetric about the vortex center-line. However, due to presence of the delta wing, the vortex is skewed. As we will see later on, the viscous core is not axisymmetric. However, to simplify our calculations, the flowfield is assumed to be axisymmetric. In subsequent studies 3-D measurements will be conducted to verify the validity of the axisymmetric assumption.

The radius of the viscous subcore, r_c, can be derived from the swirl velocity. The viscous subcore radius is defined as the distance from the vortex centerline to the point of maximum swirl velocity, $V_{\theta(max)}$ (figure 2). The viscous subcore is the region where most of the streamwise vorticity is confined. Up to 95% of the streamwise vorticity is contained inside the viscous subcore.

The swirling motion of the leading-edge vortices can also be characterized by the distribution of circulation, $\Gamma = 2\pi r V_\theta$. The circulation has a parabolic behavior near the axis and tends towards a constant value Γ_o in the outer part of the flowfield. However, since vorticity is continuously being fed into the vortex by the delta wing leading-edge, Γ_o will vary both in the axial and radial direction.

A common parameter used to describe the swirling motion is the swirl angle θ, where

$$\theta = \tan^{-1}\left(\frac{V_\theta}{V_x}\right) \qquad\qquad (1)$$

The swirl angle depends on the angle of attack, the sweepback of the wing, and the yaw angle. In general, the swirl angle increases with the angle of attack, decreases with sweepback angle, and increases with yaw (Werlé 1971). The swirl angle is an important parameter, as many studies with vortex tubes have found that breakdown generally occurs when the swirl angle reaches a

critical value (typically greater than 45 degrees) at some point. Figure 3 shows typical variations of swirl angle and circulation with radial distance from the vortex centerline. The swirl angle is zero at the center of the vortex core and reaches a maximum at the edge of the subcore, where the swirl velocity is maximum.

During vortex breakdown, since there is an abrupt change in the structure of the vortex core with rapid expansion of core size, there is also a rearrangement of the spatial distribution of vorticity. By assuming axisymmetric flow, the axial, azimuthal, and radial components of vorticity in cylindrical coordinates-Ω_x, Ω_θ, and Ω_r-can be computed from the axial and swirl velocities:

$$\Omega_x = \frac{V_\theta}{r} + \frac{\partial V_\theta}{\partial r} \qquad (2)$$

$$\Omega_\theta = \frac{\partial V_r}{\partial x} - \frac{\partial V_x}{\partial r} \approx -\frac{\partial V_x}{\partial r} \qquad (3)$$

$$\Omega_r = -\frac{\partial V_\theta}{\partial x} \qquad (4)$$

Ω_r is generally very small. Further, since V_r is normally very small as compared to $\frac{\partial V_x}{\partial r}$, the

swirl or azimuthal vorticity, Ω_θ, can be approximated by eliminating $\frac{\partial V_r}{\partial x}$. Figure 4 shows the

vorticity components calculated from the velocity profiles in figure 1. Since the swirl velocity does not change much during transition to breakdown, axial vorticity remains high in the vortex centerline. The majority of the axial vorticity is contained within the vortex subcore. On the other hand, we observe that in the transition to breakdown, the swirl vorticity component changes

sign with breakdown. The highest values of Ω_θ occur where $\frac{\partial V_x}{\partial r}$ gradients are the largest.

When there is no vortex breakdown, the axial velocity profile is jet-like and $\frac{\partial V_x}{\partial r}$ is always

negative, hence positive Ω_θ. However, when vortex breakdown occurs, axial velocity profile is

wake-like with a deficit in the center part, and $\frac{\partial V_x}{\partial r}$ is positive inside the vortex core, thus

negative Ω_θ. The significance of the production of negative swirl vorticity will be discussed further in sections below.

4. VORTEX BREAKDOWN MECHANISM

4.1 Vorticity Transport

The vortex breakdown mechanism may be simplified and explained by the concept of vorticity transport developed by Reynolds and Carr (1985). They proposed that in order for the leading-edge vortices to remain steady, it is necessary that the axial convection of vorticity along the vortex core balances the influx of vorticity generated by the separation of the leading-edge boundary layer. Vortex breakdown can be partially explained as a disturbance of the vorticity balance due to a reduction of the axial convection of vorticity.

A characteristic measure of the balance between vorticity influx and convection is the swirl angle. If the angle of attack is increased the swirl velocity increases as well. Simultaneously, axial convection of vorticity decreases because of the imposed strong adverse pressure gradient at the trailing edge resulting from the Kutta condition. Consequently, the axial location of breakdown moves closer to the apex with increasing angle of attack. The same trend was observed with smaller sweepback angles and increased yaw. Studies with vortex tubes have found that breakdown occurs when the swirl component of the flow was sufficiently large, typically when the swirl angle is above 45 degrees (i.e., when the swirl velocity exceeds the axial velocity). In terms of vorticity balance, a large swirl angle indicates that the vorticity generated at by the leading-edge separation is not been convected effectively due to the decreased axial velocity.

We can gain insight into the mechanism for initiating vortex breakdown by examining vorticity transport for the simplest case. The vorticity transport equation is:

$$\frac{D\vec{\Omega}}{Dt} = \left(\vec{\Omega} \cdot \nabla\right)\vec{V} + \nu\nabla^2\vec{\Omega} \qquad (5)$$

ignoring viscosity, the axisymmetric vorticity transport equation in the azimuthal direction is:

$$\frac{\partial \Omega_\theta}{\partial t} + V_r \frac{\partial \Omega_\theta}{\partial r} + \frac{V_\theta}{r}\frac{\partial \Omega_\theta}{\partial \theta} + \frac{V_r \Omega_\theta}{r} + V_x \frac{\partial \Omega_\theta}{\partial x} = \Omega_r\left(\frac{\partial V_\theta}{\partial r}\right) + \Omega_\theta\left(\frac{1}{r}\frac{\partial V_\theta}{\partial \theta} + \frac{V_r}{r}\right) + \Omega_x \frac{\partial V_\theta}{\partial x} \quad (6)$$

For the simplest case, assume that V_r and Ω_r are small, $V_\theta = V_\theta(x,r)$, $V_x = V_x(r)$, we get

$$\frac{\partial \Omega_\theta}{\partial t} = \Omega_x \frac{\partial V_\theta}{\partial x} \qquad (7)$$

Equation (7) describes the temporal development for the redistribution of the axial vorticity Ω_x into the swirl vorticity component Ω_θ, if the swirl velocity component decreases in the axial direction x, Ω_θ is negative and will decrease with time. If $\Omega_\theta < 0$, the swirl vorticity distribution will induce an axial velocity component u_{ind} opposite to the main flow direction due to the Biot-Savart law. This causes a strong deceleration of the axial velocity component.

4.2 Positive feedback Mechanism

The positive feedback mechanism for breakdown in pipes has been proposed. A positive axial pressure gradient at large radial distances from the axis of the slender vortex leads to a deceleration of the axial velocity component. Conservation of mass requires radial outflow and from the conservation of angular momentum and the vorticity transport equation, a redistribution of the axial vorticity component into the azimuthal vorticity component follows. The azimuthal vorticity component induces an additional axial velocity component against the main flow direction, resulting in an even stronger deceleration of the axial velocity, and therefore enhancement of the radial velocity component. This feedback amplifies the redistribution of the axial vorticity into the azimuthal vorticity. This process may lead to the formation of a stagnation point on the axis of the slender vortex, followed by a region of recirculating flow.

Brown and Lopez (1990) were the first to note the positive feedback loop for the initiation of bubble-type vortex breakdown in a pipe. The above argument can also be made for the development of the vortex lines: If the flow on the axis of a slender vortex is decelerated, conservation of mass requires radial outflow. The vortex lines, which are straight and parallel upstream of the point of deceleration, are stretched and tilted in the region of radial outflow. The tilting of the axial vorticity is a consequence of the conservation of circulation along a stream surface in steady, inviscid flow. The vorticity vector $\bar{\Omega}$ acquires a component in the azimuthal direction, and the axial flow is decelerated due to induction. Stretching and tilting of the vortex lines are further enhanced. This nonlinear interaction between stretching and tilting and

6

deceleration of the axial flow may be promoted by a positive axial pressure gradient at large radial distances. The interaction may cause an upstream migration of the stagnation point leading to either a stable vortex or a bubble- or spiral-type breakdown. The mechanism is assumed to be purely inviscid and relies upon a radial outflow or, equivalently, an adverse pressure gradient, to drive the breakdown process.

In the absence of viscous or turbulent diffusion, Brown and Lopez postulated that a necessary condition for vortex breakdown to occur is that the helix angle for the velocity exceeds that of the vorticity on some stream surfaces. That is, on some stream surfaces, $\dfrac{V_\theta}{V_x} > \dfrac{\Omega_\theta}{\Omega_x}$.

4.3 Inviscid or Viscous Mechanism

In general, most theoretical studies of vortex breakdown may be classified into the following categories:

1. Quasi-cylindrical approach and analogy to two-dimensional boundary layer separation (Hall 1965).

2. Hydrodynamic instability (Ludwieg, 1962).

3. Wave-motion theories:
   a. Finite transition between critical states, analogous to a hydraulic jump (Squire 1960, Benjamin 1962).
   b. Breakdown is the result of the trapping of long, weakly nonlinear wave propagating in nearly critical swirling flows (Randall and Leibovich 1973).
   c. Two-stage transition (Escudier and Keller 1983).

Flow visualization has shown that the structure and location of the leading-edge vortices is independent of the Reynolds number (Lee and Ho, 1990). This seems to imply that the breakdown is governed by an inviscid mechanism. However, the detailed flow structure, such as the location and strength of the secondary flow separation, depends on whether the leading edge is sharp or round. Furthermore, the viscous core of the leading edge vortices decreases in size with increasing Reynolds number due to the thinning of the boundary layer at the leading edge. In addition, while a few inviscid theories may invoke viscosity to initiate breakdown, all inviscid theories contend that the rapid transformation of the vortex cannot be attributed to viscosity. It is rather a result of inertial effects such as instability or wave propagation.

7

On the other hand, viscous theories point to the slenderness of the vortex subcore and argue that viscous forces play the dominant role for its generation. Since the subcore is slender, viscous diffusion could occur rapidly. Using the analogy to two-dimensional boundary layer separation, since the gradients of vorticity becomes increasingly large towards the vortex axis, it is expected that viscous diffusion could become appreciable. By feeding the outer inviscid solution into the full Navier-Stokes equation and comparing the inertial and viscous terms, Hall (1965) argues that inside the subcore viscous forces are as important as inertial forces. The governing equations demonstrates that the interplay between radial inertial, pressure, and viscous forces are important inside the subcore (Berger and Erlebacher 1995). Consequently, some argues that breakdown is necessarily a viscous phenomenon.

Experimental results that can shed more light on the validity of these theories are not available as the flow regime is three-dimensional and involves large flow gradients within a small region. Hence any measurement technique has to be not only non-intrusive but also sufficiently accurate to resolve the important flow features. Furthermore, since vortex breakdown is an axially evolving flow field, measurements would need to be taken at several axial locations with accurate spatial resolution.

The above problems were overcomed in the present work on a delta wing in unsteady free stream. In this novel approach, in addition to the spatial domain, the mechanism of vorticity transport over a delta wing was analyzed in the temporal domain by varying the upstream production of leading-edge vorticity. This enables the study of vortex breakdown both in the spatial and the temporal domain. In addition, this allows the breakdown process to be studied in its most fundamental definition--the failure of the fluid to transport vorticity in an organized and efficient fashion. As the upstream leading-edge vorticity underwent large amplitude oscillations, the vorticity transport within the core changed as well, even to the point of breakdown. The problem thus provided the means for ascertaining whether the dominant mechanism of breakdown was viscous or inviscid. If viscous diffusion were to be the dominant mechanism of breakdown, then the vorticity transport through the vortex core would be sharply different during and after breakdown. On the other hand, if the breakdown mechanism was inviscid, there will be no sharp change during and after breakdown as the vortex core would still continue to transport

vorticity through fluid convection. In essence, the inviscid mechanism would require a unique relation between the fluid flow rate and the fluid circulation within the vortex core.

5. VORTEX BREAKDOWN IN UNSTEADY FREE STREAM

5.1 Unsteady Flow Field

All experiments were conducted in the unsteady water channel at UCLA. The freestream velocity varies as:

$$\frac{V_x}{U_\infty} = 1 + R\cos\omega t = 1 + R\cos\frac{2\pi t}{T} \tag{8}$$

where U_∞ is the time-averaged freestream velocity, R is the dimensionless amplitude ($R<1$), and $\omega=2\pi/T$ is the radial frequency of the velocity variation. The reduced frequency can be defined as $k=\omega c/2U_\infty$, and is the ratio between the vortex convection time-scale (c/U_∞) and the external perturbation time scale ($2\pi/\omega$).

The global feature of the vortex breakdown phenomenon was examine by flow visualization for both the steady and unsteady cases. Aspect ratio 1, 2 and 4 (sweep back angle 76 deg, 63.4 deg, and 45 deg respectively) delta wings were studied at different angle of attack. Vortex breakdown depends both on the angle of attack and the sweep back angle. For a given sweep angle, vortex breakdown takes place near the trailing edge and moves upstream with increasing angle of attack (note steady free stream pictures in figure 5). At the same angle of attack, larger sweep angles delays the occurrence of breakdown at the trailing edge. For a given angle of attack and sweep angle, when steady breakdown position is near the midcore and the trailing edge, unsteady forcing can cause the breakdown position to vary by large amplitudes, as large as 40-50% of the chord length during an unsteady cycle (cf. figure 5 (a) and (b) for $\alpha=15$ and 20 degrees). However, for very small and very large angle of attacks, i.e., when the steady breakdown position is very far downstream or near the apex, vortex breakdown locations varies very little during unsteady forcing (figure 5 (d) and (e), $\alpha=30$ and 40 degrees).

For the cases where there is large variation of the vortex breakdown position during unsteady forcing, flow visualization shows that the breakdown positions moves downstream

during flow deceleration ($0 \leq t/T \leq 0.5$), but suddenly appears at an upstream location during flow acceleration (figure 5 (b), $A=2$, $\alpha=20$ degrees, $k=0.766$, $R=0.583$, $t/T{\sim}0.75$), and then moves downstream. This implies that the axial velocity is undergoing a change in flow property.

To verify this transition, detailed velocity field measurement were conducted along a plane across the vortex core for an aspect ratio one delta wing. Measurements of velocity components parallel and normal to the wing surface were taken in the plane containing the vortex core axis. Since the measurements were taken along a traverse line parallel to the trailing edge, the velocity components measured approximately correspond to the axial and swirl velocities across the vortex core. Phase-averaged measurements were taken at different streamwise locations for $\alpha=15$ degrees, amplitude $R=0.42$, and reduced frequency $k=1.27$. The origin of the coordinate system is located at the trailing edge and centered about the vortex core. Figure 6 shows the spatial variation of axial velocity through an unsteady cycle. When breakdown occurs over the wing, the axial velocity distribution shows an abrupt transition from a jet-like to a wake-like profile at the breakdown location. During flow deceleration ($0<t/T<0.5$), breakdown moves downstream beyond the trailing edge of the delta wing. After the breakdown leaves the wing, axial velocity profile everywhere on the wing is jet-like ($t/T=0.375$), with velocity close to two times the freestream velocity. At $t/T=0.875$, axial velocity is almost uniform everywhere along the wing. Axial velocity profiles then transform to wake-like at most axial locations after this instant. Figure 6 verifies that by varying the freestream velocity, we can manipulate the vortex breakdown position as to enable the study vortex breakdown not only in the spatial domain, but also the temporal evolution of breakdown.

As we have noted in figure 1 , the swirl velocity profile does not change much through the breakdown process. This is evident in the swirl velocity surveys (figure 7) during flow deceleration and acceleration. The swirl velocity profile remains similar spatially even during transition between no-breakdown and breakdown. Note that the second band of high velocity region beyond $r \sim 16$ mm is already beyond the outer edge of the delta wing leading-edge, thus velocity field in that region approximates the normalized freestream value. Figures 8 is the same velocity profiles of figures 6 and 7 plotted in vector form.

The swirl velocity can be used to determine the radius of the vortex viscous subcore (cf. Figure 2). Figures 9 shows the variation of the vortex viscous subcore radius during the unsteady cycle. As expected, when breakdown occurs, the subcore expands in size, and vice versa.

Studies with vortex tubes have found that breakdown occurs when the swirl component of the flow was sufficiently large, typically when the swirl angle is above 45 degrees (i.e., when $V_\theta > V_x$). Contrary to those studies, the present data shows that the swirl angle is not a good indicator of breakdown when the flow is unsteady (figure 10). Comparing axial velocity distributions with swirl angle, there is no direct correlation between maximum swirl angle and vortex breakdown. In fact, the highest swirl angle occurs at time intervals where there axial velocity is jet-like everywhere in the plane (t/T=0.375).

Since dramatic changes take place in the vortex core during the breakdown process, its effect on global quantities such as circulation is of primary interest. Ng (1989) proposed that the vortex may have a limit on the maximum amount of vorticity per unit area at a given station. Consequently, a critical vorticity concentration occurs above which the aerodynamic forces cannot maintain a stable vortex over the airfoil. If this concentration is exceeded, the vortex transitions to another state, such as post breakdown, to redistribute the excess vorticity. In other words, the local flow condition around breakdown is similar to that of a two-dimensional airfoil during static stall. For example, an increase in the angle of attack leads to a higher rate of generation of the axial vorticity component without an accompanying increase in the axial velocity. The subsequent increase in the vortex strength, therefore, leads to vortex breakdown. However, figure 11 shows that the circulation is not influenced by the breakdown, as the profiles seems to be similar and varies with freestream velocity variation.

Axial vorticity calculations (Figure 12) shows that most of the vorticity is contained within the vortex viscous subcore, and varies very little with breakdown. This is expected since the swirl velocity does not give indication of breakdown. Therefore, simply determining the maximum value of the axial vorticity does not make a definitive statement of the status of the vortex.

The Brown-Lopez hypothesis argues that the breakdown mechanism relies on the production of negative azimuthal vorticity. This results from a tilting and stretching of the predominantly axial vorticity vector Ω_x. During breakdown, the mean rotational vector $\bar{\Omega}$ changes from an

11

essentially axial direction to a generally tangential direction during breakdown. Figure 13 shows the production of negative azimuthal vorticity in the regions where breakdown occurs (cf. figure 6).

To better examine how the vorticity is being redistributed during breakdown, the amount of vorticity has been computed by integrating the axial and azimuthal vorticity ($\Sigma \Omega A / c U_\infty$) in the inner region (-16 < r < 16 mm). Since most of the vorticity is contained in the viscous subcore, and the subcore radius is always less than 16 mm, the integrated vorticity values will give us an idea of the total amount of vorticity flux. Figure 14 shows the temporal variation of the integrated vorticity at different streamwise locations. The dash lines denote negative vorticity. It can be clearly seen that when breakdown occurs, the vorticity has been distributed from the axial component to the production of azimuthal vorticity. Furthermore, at the upstream position where breakdown does not occur (X = -100 mm), the axial vorticity varies as the freestream velocity. However, at the downstream position (X = 0 mm), there is a phase shift of the integrated vorticity values with freestream velocity. This is due to the delay caused by the vortex convection from the leading-edge. This will be discussed in more detain in the section below. In addition, it is difficult to correlate between breakdown and the maximum amount of vorticity, as the present data does not provide evidence to support the argument that breakdown occurs as a result of a total amount of vorticity being reached at a given streamwise position.

In addition to the rotation of the vorticity vector and the production of negative azimuthal vorticity, Brown and Lopez postulated that a necessary condition for vortex breakdown to occur is when the helix angle for the velocity exceeds that of the vorticity on some stream surfaces, i.e.. $\frac{V_\theta}{V_x} > \frac{\Omega_\theta}{\Omega_x}$. Figure 15 shows the Brown and Lopez criterion at different phases of the unsteady cycle. The criterion has been dichotomized such that $\frac{V_\theta}{V_x} > \frac{\Omega_\theta}{\Omega_x}$ is shown in white and $\frac{V_\theta}{V_x} < \frac{\Omega_\theta}{\Omega_x}$ is shown in black. Comparing with the radius of the vortex subcore (figure 9), we find that the Brown-Lopez criterion is globally satisfied inside the vortex subcore only just before breakdown (t/T=0.875). The criterion holds true at all radial locations inside the subcore only at t/T=0.875 and not at any other instant. In the outer flow region, the gradients of axial and swirl

velocities are small, thus susceptible to large errors when computing and comparing vorticity ratios. Consequently for the present case we can only verify the Brown-Lopez condition inside the subcore, where the velocity gradients are large. Nevertheless, our present data does verify the validity of the Brown-Lopez condition inside the vortex subcore.

5.2 Unsteady Vortex Breakdown Mechanism

The organization of the unsteady flowfield can also be revealed by examining the streamlines, which are defined as iso-value lines of the stream function $\Psi(X,r)$, where,

$$\Psi(X,r) = \int_0^r \frac{V_x}{U_\infty} \eta d\eta \qquad (9)$$

Further, since the flowrate for axisymmetric flow is defined as $Q_m(X,r)$, where

$$Q_m(X,r) = 2\pi \int_0^r \frac{V_x}{U_\infty} \eta d\eta \qquad (10)$$

the streamlines also represent the constant-mass flow lines. Figure 16 shows the unsteady flow streamlines. The constant-mass flow lines have been normalized by the maximum mass-flow rate at the outer flow. Each successive streamline outwards from the vortex center ($r=0$) has twice the mass-flow rate as the previous one. Throughout the unsteady cycle the streamlines stay straight and parallel in the axial direction, verifying that the vortex flow is quasi-cylindrical. When there is breakdown over the delta wing (the duration from $t/T=0.875$ to 1.250), there is slight divergence of the streamlines along the axial locations where breakdown is occurring. Conservation of mass requires this radial outflow due to axial velocity deceleration. To see how the flow rate is evolving in the time domain, figures 17 examine how the flow rate changes at each axial location during the unsteady cycle. Again, at the axial locations where breakdown occurs, the constant-mass flow rate contract and expands with upstream flow condition. Figure 18 shows the temporal variation of vortex viscous core size (r_c) at different axial locations. The viscous subcore size expands and contract in temporally in response to breakdown and upstream velocity variations.

The temporal evolution of circulation (figure 19) also shows that the lines of constant circulation at any give location contract and expand rhythmically. To get a better picture of how the circulation at a fixed radial position changes with time, the figure 19 has been replotted as

13

surface plots at selected axial locations (figure 20). The circulation at any radial distance from the vortex core exhibits cyclical variation with time. Beyond $r \sim 20$ mm, the measurements are already beyond the outer leading-edge of the delta wing, thus the circulation varies in phase with the freestream velocity. However, as we move inward towards the vortex core, the variation of circulation has a phase-lag with the free stream. This delay is clearly a result of the time it takes for the upstream vorticity to convect inside the core. Vorticity balance concept dictates two time scales when the freestream velocity is unsteady. First, the change in the vorticity generation along the leading-edge due to the unsteady freestream is transmitted into the core in one local vortex turn-over time (the characteristic time for one local revolution of the vortex). For our case, we can say that this turn-over time is closely related to our flow forcing time scale ($2\pi/\omega$). This time is minimal at the apex, and increases towards the trailing edge. Therefore, the flow around the apex is more sensitive to disturbances than at any other location along the leading edge. This explains that why flow visualization shows that at high angle of attack, when the breakdown is near the apex, often asymmetric vortices are observed over the wing (figure 5 (d)). The second time scale is determined by the time during which an upstream disturbance is convected throughout the vortex. This characteristic time is c/U_∞, where c is the mean chord of the delta wing and U_∞ is the average freestream velocity. This relationship can be represented by the reduced frequency. Since, in general, the vortex convection time scale is longer than the local turn-over time (for our case $k=1.27$), streamwise convection becomes the limiting factor for the vortex to respond to any disturbance. Because of the streamwise convection time, a phase lag of response occurs relative to the freestream velocity variation. This is what we observe in figure 20.

It is interesting to note that the viscous core size expands and contracts by rather large amplitude with time (figure 18). However, despite the increase in the vortex core size, the flow rate and circulation do not show corresponding large variation. If viscous diffusion was responsible for transporting the vorticity outwards, we should see circulation and flow rate change as well. This seem to imply that most of vorticity is being convected away. Further, although the flow rate does not show very big change, figures 17 and 19 show that the flow rate and circulation vary in phase as the upstream vorticity and velocity changes with time. This demonstrates that vorticity is convecting with the fluid particles both before and after

14

breakdown. If viscous diffusion were to have played a dominant role during breakdown, then the circulation profile should show a difference from the profile for flow rate. The absence of any such deviation leads to the conclusion that vortex breakdown is an inviscid mechanism.

6. FUTURE DIRECTIONS

Previous studies of vortex breakdown have tried to formulate and quantify flow properties as to correlate with breakdown. It was generally thought that breakdown occurs when certain parameters reaches some critical value, such as the swirl angle or the amount of vorticity. As we have shown for unsteady flows, vortex breakdown is an extremely complex phenomenon and cannot be characterized by any single parameter. Vortex breakdown mechanism involves the local properties of the fluid velocity distributions, as well as global properties such as circulation and flow rate.

Although much can be understood from a single cut through the vortex core, more work is needed to evaluate the three-dimensional flowfield to examine the global influence of vortex breakdown. In the present studies we have assumed that the radial components of velocity and vorticity is small. However, that assumption might not be valid when breakdown occurs. To really clarify the role of viscous diffusion inside the vortex subcore, full three-dimension velocity and vorticity fields will have to be considered. The Brown-Lopez criterion relies on the assumption that the initial reduction in the azimuthal component of vorticity to be due to viscous diffusion and the resultant stretching and tilting of axial vorticity. As the flow begins to diverge, the further production of negative azimuthal vorticity is dominated by inviscid mechanisms. Detailed three dimensional data inside the vortex core will enable us to solidify the breakdown mechanism.

7. PERSONNEL

Principal Investigator: Dr. Ho, Chih-Ming

Post-Doctoral Research Associate: Dr. Srinivasan Subramanian

Post-Doctoral Research Associate: Dr. Yitshak Zohar

Research Assistant: Mr. Hank Lin

Graduate Student: Mr. Chris Pettit, Jr.
M.S. in Aerospace Engineering, UCLA, December 1992.
Thesis Title: Loads on a Pitching Delta Wing

Graduate Student: Mr. Jack Yoh

8. PUBLICATIONS

Gursul, I., and Ho, C. M., "High Aerodynamic Loads on an Airfoil Submerged in an Unsteady Stream," *AIAA Journal*, Vol. 30, No. 4, April 1992, pp. 1117-1119.

Lin, H., and Ho, C. M., "Optical Pressure Transducer," *Review of Scientific Instruments*, Vol. 64, No. 7, July 1993, pp. 1999-2002.

Shih, C., and Ho, C. M., "Vorticity Balance and Time Scales of a Two-Dimensional Airfoil in an Unsteady Free Stream," *Physics of Fluids*, Vol. 6, No. 2, Pt. 2, February 1994, pp. 710-723.

Gursul, I., and Ho, C. M., "Vortex Breakdown over a Delta Wing in Unsteady Free Stream, *AIAA Journal*, Vol. 32, No. 2, February 1994, pp. 433-436.

Gursul, I., Lin, H., and Ho, C. M., "Effects of Time Scales on Lift of Airfoils in an Unsteady Stream," *AIAA Journal*, Vol. 32, No. 4, April 1994, pp. 797-801.

Gursul, I., Lin, H., and Ho, C. M., "Parametric Effects on Lift Force of an Airfoil in Unsteady Free Stream," Accepted for publication in *AIAA Journal*.

9. CONFERENCES AND WORKSHOPS

Gursul, I., "Vortex Breakdown in Unsteady Flow," AFOSR Workshop on Supermaneuverability: Physics of Unsteady Flows Past Lifting Surfaces at High Angle of Attack, Lehigh University, April 9-10, 1992.

Ho, C. M., Lin, H., and Gursul, I., "Delta Wings in Unsteady Flows," Proceedings of the Fifth Asian Congress of Fluid Mechanics, Vol. 2, Taejon, Korea, August 10-14, 1992, pp. 823-826.

Gursul, I., and Ho, C. M., "Vortex Breakdown over Delta Wings in Unsteady Free Stream," AIAA Paper 93-0555, 31th Aerospace Sciences Meeting, Reno, NV, January 11-14, 1993.

10. REFERENCES CITED

Benjamin, T. B., "Theory of the Vortex Breakdown Phenomenon," *Journal of Fluid Mechanics*, Vol 14, 1962, pp. 593-629.

Berger, S. A., and Erlebacher, G., "Vortex Breakdown Incipience: Theoretical Considerations," *Physics of Fluids*, Vol. 7, No. 5, May 1995, pp. 972-982.

Brown, G. L., and Lopez, J. M., "Axisymmetric Vortex Breakdown Part II: Physical Mechanisms," *Journal of Fluid Mechanics*, Vol. 221, Dec. 1990, pp. 553-576.

Escudier, M. P., and Keller, J. J., "Vortex Breakdown: A Two-Stage Transition," AGARD CP No. 342, *Aerodynamics of Vortical Type Flows in Three Dimensions*, Paper 25, 1983.

Hall, M. G., "A Numerical Method for Solving the Equations for a Vortex Core," Aeronautical Research Council R & M, No. 3467, 1965.

Lee, M., and Ho, C. M., "Lift Force of Delta Wings," *Applied Mechanics Reviews*, Vol. 43, No. 9, September 1990, pp. 209-221.

Ludwieg, H., "Zur Erklarung der Instabiliat der uber angestellten Deltaflugeln aufretenden freien Wirbelkerne," Z. Flugwiss, Vol. 10, 1962, pp. 242-249.

Ng, T. T., "On Leading Edge Vortex and Its Control," AIAA Paper 89-3346, Boston, MA, Aug. 1989.

Peckham, D. H., and Atkinson, S.A., "Preliminary Results of Low Speed Wind Tunnel Tests on a Gothic Wing of Aspect Ratio 1.0," Aeronautical Research Council Technical Report C.P. No. 508, TN No. Aero. 2504, 1957.

Randall, J., D., and Leibovich, S., "The Critical State: A Trapped Wave Model of Vortex Breakdown," *Journal of Fluid Mechanics*, Vol. 45, 1971, pp. 495-515.

Reynolds, W. C., and Carr., L.W., "Review of Unsteady, Driven, Separated Flows," AIAA Paper 85-0527, 1985.

Squire, H. B., "Analysis of the 'Vortex Breakdown' Phenomenon. Part 1," Imperial College of Science and Technology, Aeronautics Department Report No. 102, 1960.

Wentz, W. H., and Kohlman, D. L., "Vortex Breakdown on Slender Sharp-Edged Wings," *Journal of Aircraft*, Vol. 8, No. 3, March 1971, pp. 156-161.

Werlé, H., "Sur l'éclatement des tourbillons (On Vortex Bursting)," France Office National d'Etudes et de Recherches Aérospatiales (ONERA), Note Technique, No. 175, 1971.

11. LIST OF FIGURES

Fig. 1. Normalized velocity profiles before, transition to, and after breakdown: (a) axial velocity, (b) swirl velocity.

Fig. 2. Swirl velocity distribution: (a) behavior of swirl velocity in the inner viscous core region, (b) definition of the radius of the vortex viscous subcore r_c.

Fig. 3. Variation of flow property distribution with radial distance from the vortex center-line before, transition to, and after breakdown: (a) swirl angle, (b) normalized circulation.

Fig. 4. Variation of vorticity components calculated from velocity profiles of figure 2 before, transition to, and after breakdown: (a) axial vorticity, (b) swirl or azimuthal vorticity.

Fig. 5. Flow visualization for A=2 delta wing: (a) α=15 degrees, k=0.837, R=0.593, (b) α=20 degrees, k=0.766, R=0.583, (c) α=25 degrees, k=0.822, R=0.590, (d) α=30 degrees, k=0.822, R=0.589, (e) α=40 degrees, k=0.811, R=0.581.

Fig. 6. Normalized axial velocity survey of a plane across the vortex core centerline during an unsteady cycle: (a) deceleration; (b) acceleration. α=15 deg., A=1, k=1.27, R=0.42.

Fig. 7. Normalized swirl velocity survey of a plane across the vortex core centerline during an unsteady cycle: (a) deceleration; (b) acceleration. α=15 deg., A=1, k=1.27, R=0.42.

Fig. 8. Velocity vectors of a plane across the vortex core centerline during an unsteady cycle: (a) normalized axial velocity, (b) normalized swirl velocity. α=15 deg., A=1, k=1.27, R=0.42.

Fig. 9. Variation of vortex viscous core position during an unsteady cycle: (a) deceleration; (b) acceleration. α=15 deg., A=1, k=1.27, R=0.42.

Fig. 10. Swirl angle survey of a plane across the vortex core centerline during an unsteady cycle: (a) deceleration; (b) acceleration. α=15 deg., A=1, k=1.27, R=0.42.

Fig. 11. Normalized circulation survey of a plane across the vortex core centerline during an unsteady cycle: (a) deceleration; (b) acceleration. α=15 deg., A=1, k=1.27, R=0.42.

Fig. 12. Normalized axial vorticity survey of a plane across the vortex core centerline during an unsteady cycle: (a) deceleration; (b) acceleration. α=15 deg., A=1, k=1.27, R=0.42.

List of Figures

Fig 1. Normalized velocity profiles before (t/T=0.375), transition
to (t/T=0.875), and after (t/T=1.000) vortex breakdown.

(a) definition of the radius of the vortex viscous subcore r_c

(b) behavior of swirl velocity in the iner viscous core region.

Fig. 2. Swirl velocity distribution
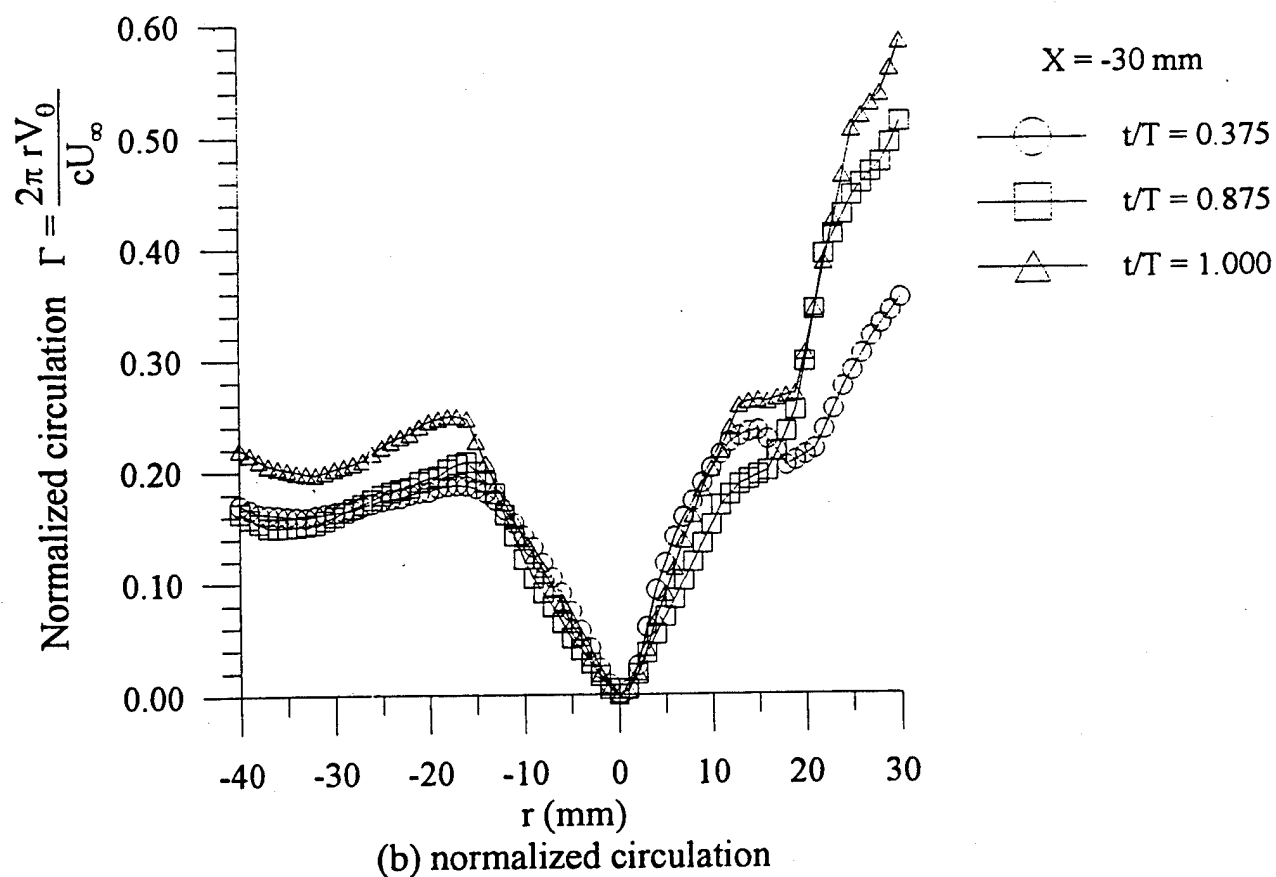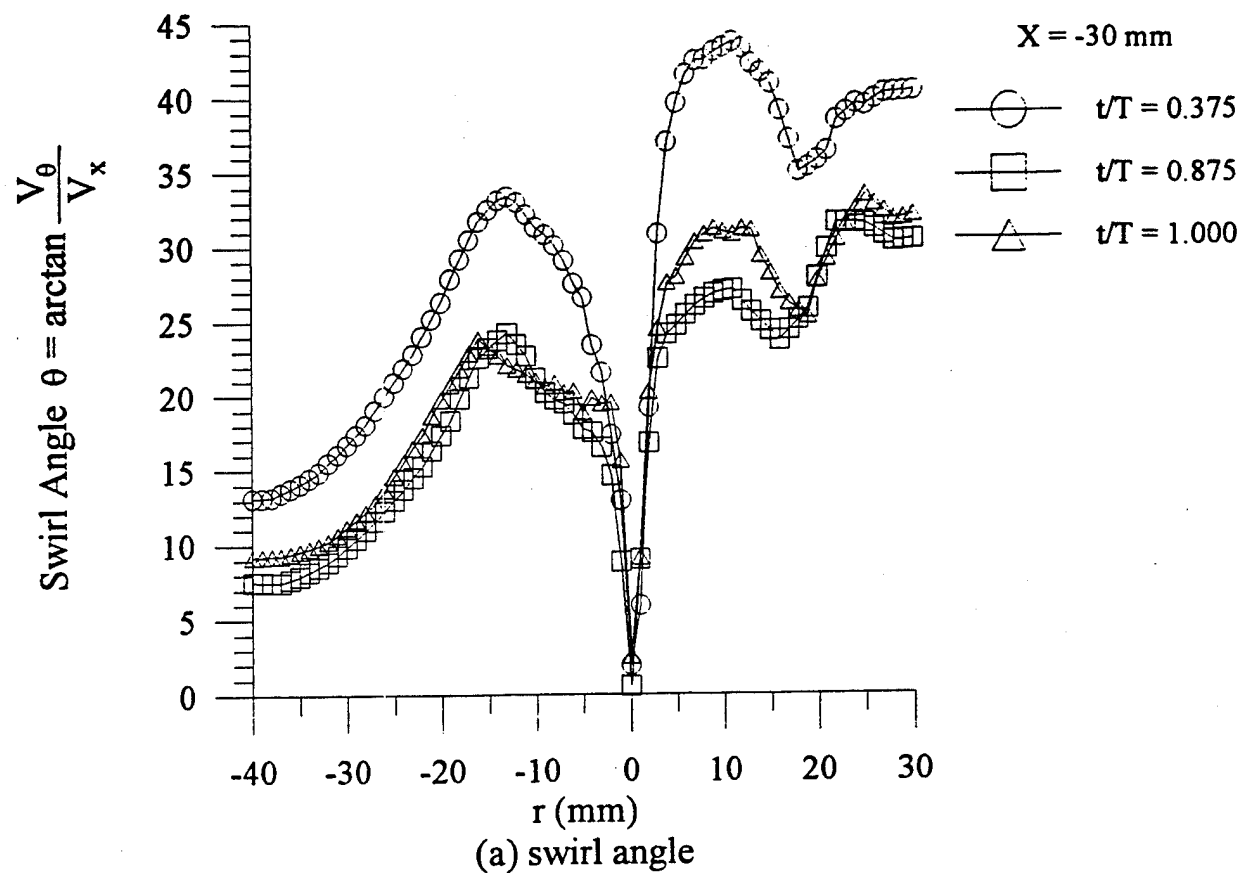
Fig. 3. Variation of flow property distribution with radial distance from the vortex centerline before (t/T=0.375), transition to (t/T=0.875), and after (t/T=1.000) vortex breakdown.
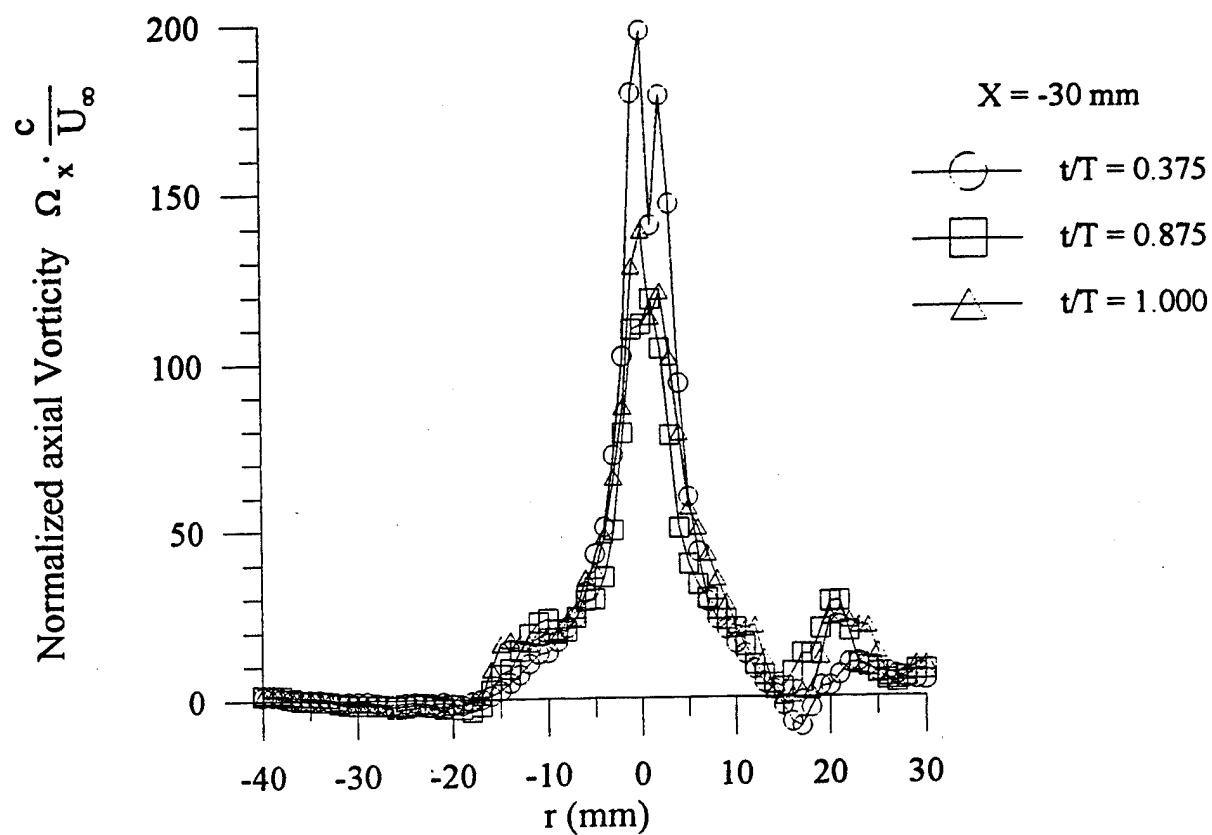
(a) normalized axial vorticity $\Omega_x \cdot \dfrac{c}{U_\infty}$
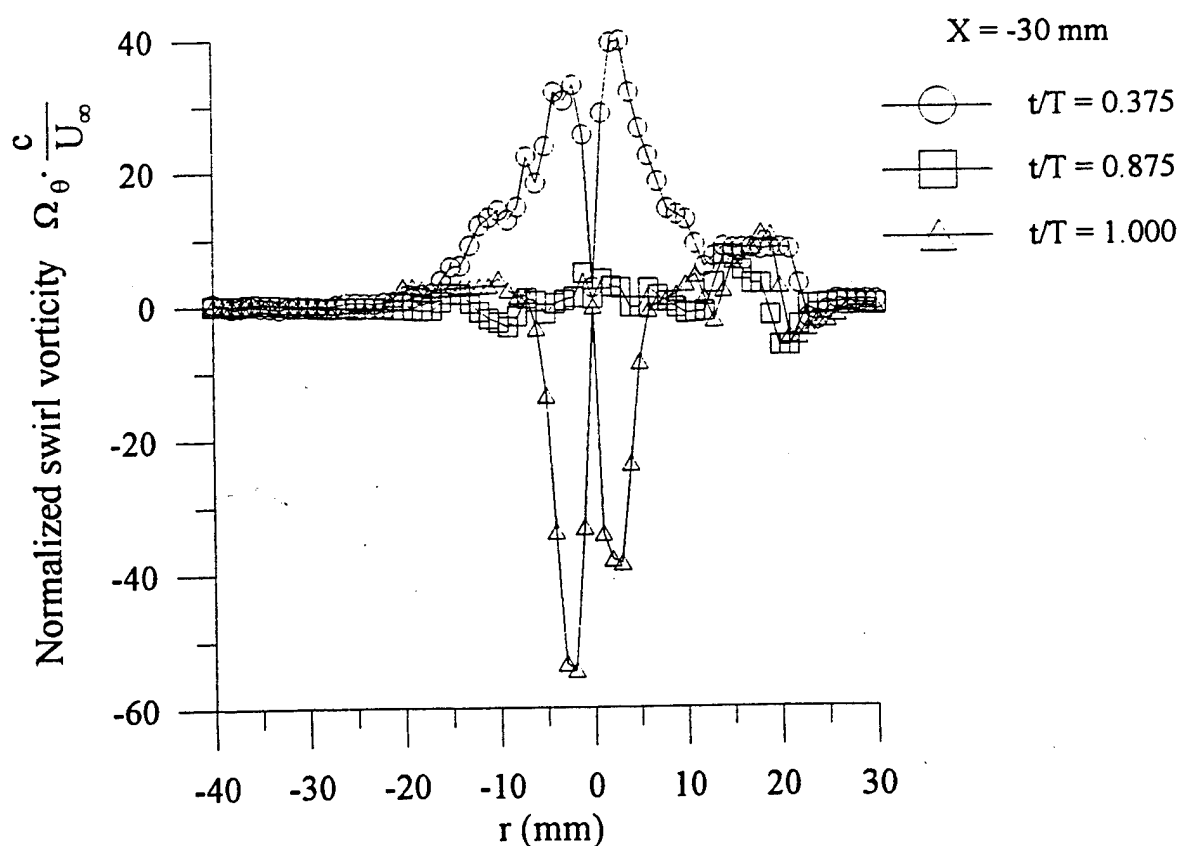
(b) normalized azimuthal vorticity $\Omega_\theta \cdot \dfrac{c}{U_\infty}$

Fig. 4. Variation of vorticity components calculated from axial velocity profiles of figure 1 before (t/T=0.375), transition to (t/T=0.875), and after (t/T=1.000) vortex breakdown.
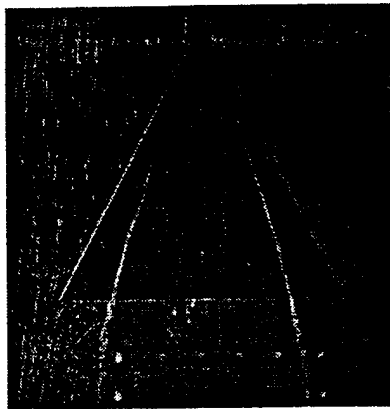
Steady free stream t/T = 0.000 t/T = 0.125
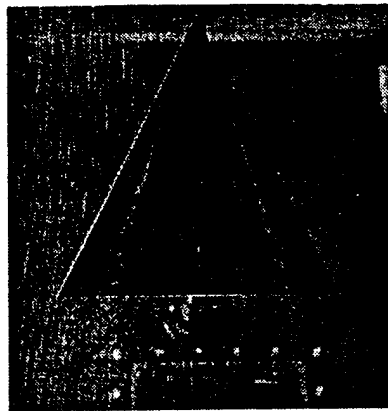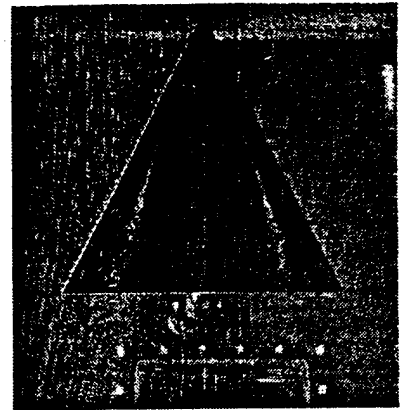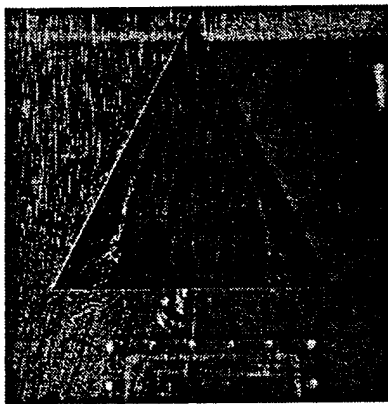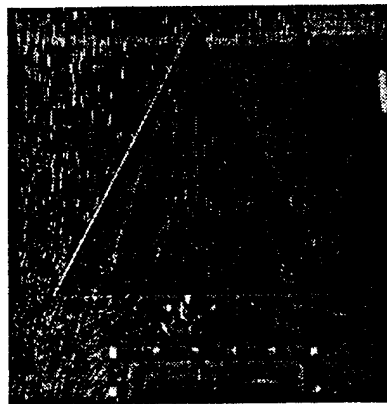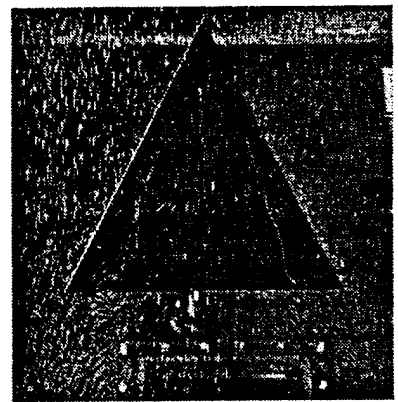
t/T = 0.250 t/T = 0.375 t/T = 0.500
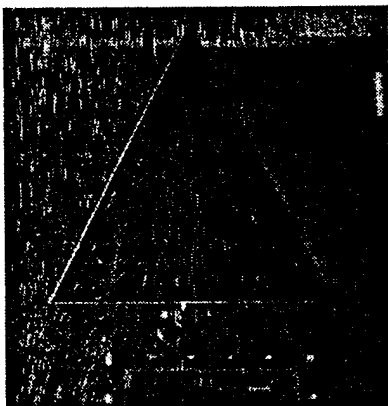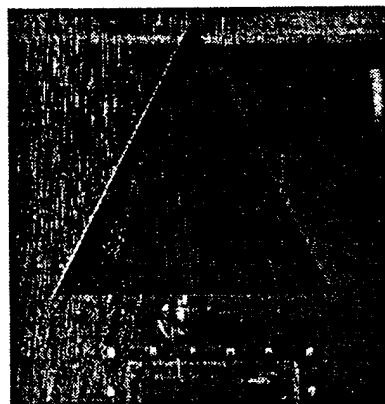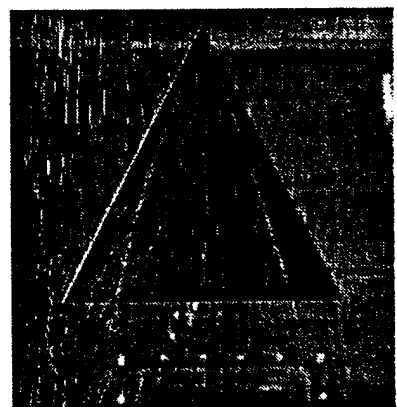
t/T = 0.625 t/T = 0.750 t/T = 0.875

Fig. 5 (a). Flow visualization for A = 2 delta wing, α = 15 deg, k = 0.837, R = 0.593.
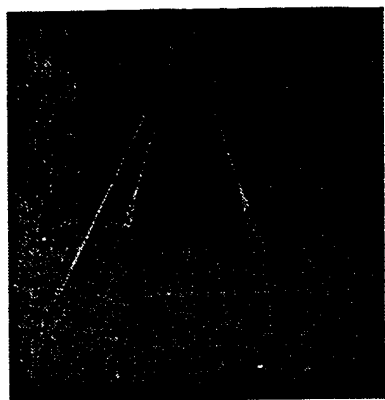
Steady free stream
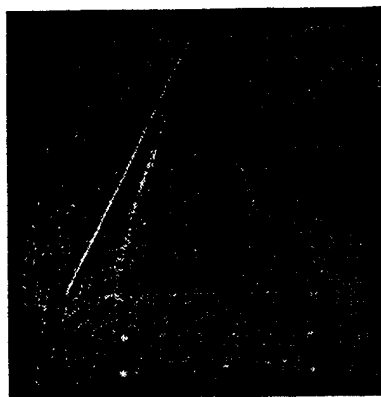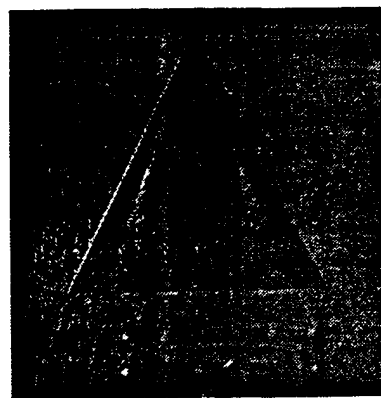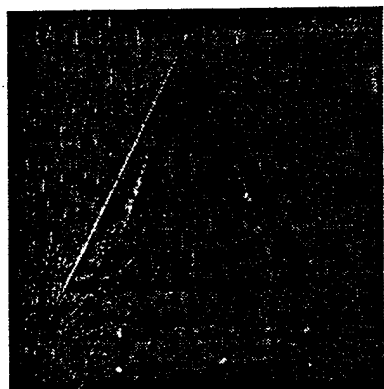
t/T = 0.000
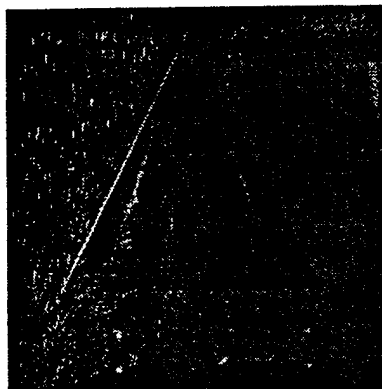
t/T = 0.125
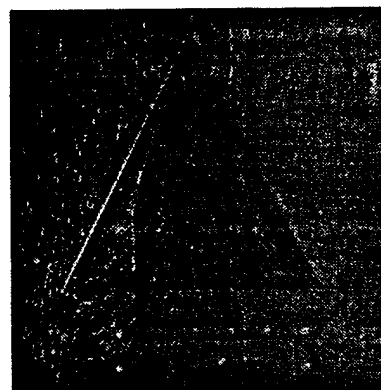
t/T = 0.250
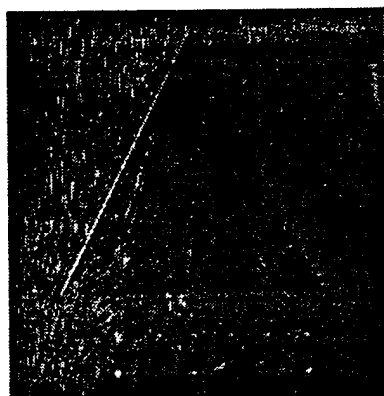
t/T = 0.375
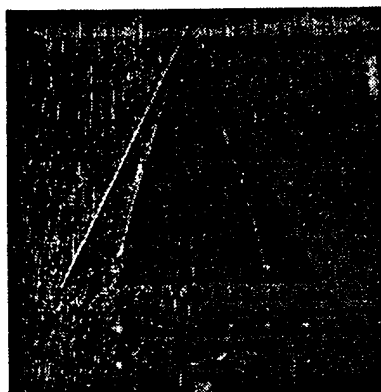
t/T = 0.500
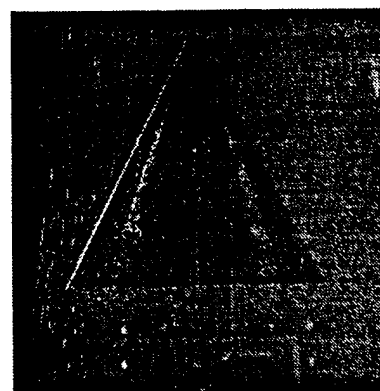
t/T = 0.625

t/T = 0.750

t/T = 0.875

Fig. 5 (b). Flow visualization for A = 2 delta wing, α = 20 deg, k = 0.766, R = 0.583.
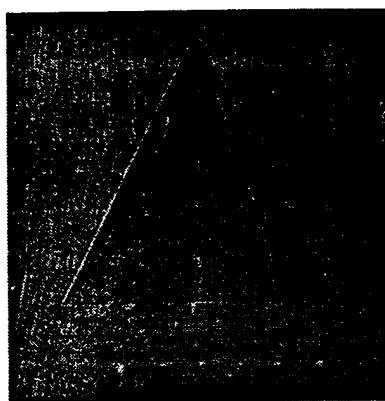
Steady free stream
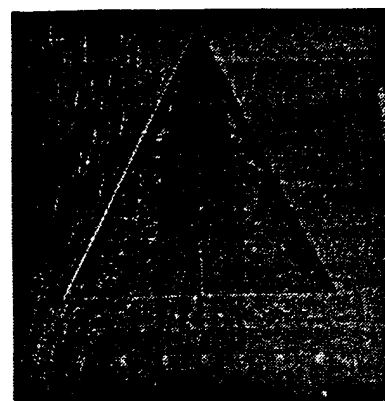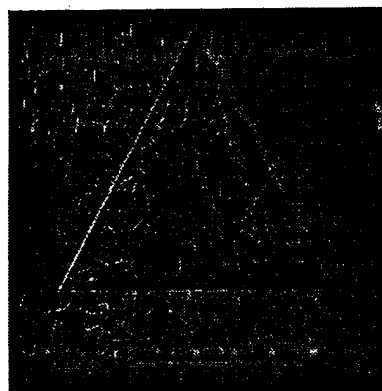
t/T = 0.000
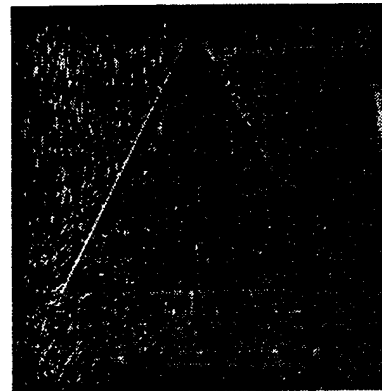
t/T = 0.125
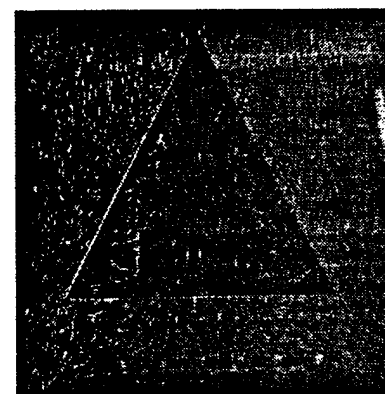
t/T = 0.250
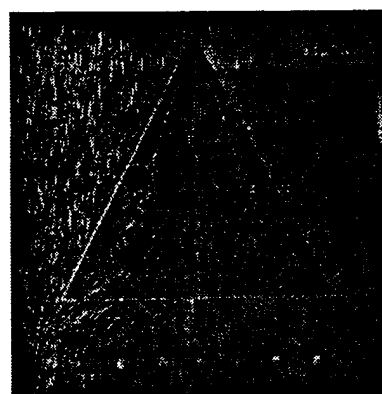
t/T = 0.375
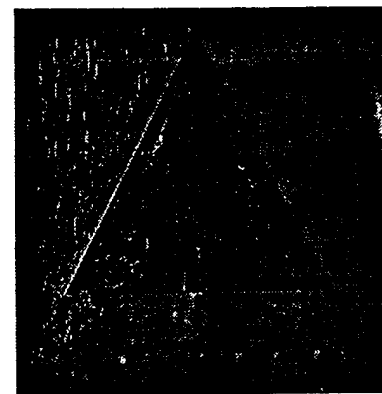
t/T = 0.500
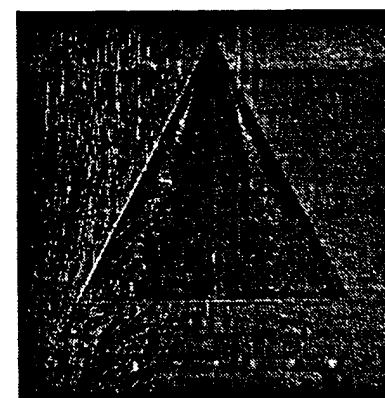
t/T = 0.625

t/T = 0.750

t/T = 0.875

Fig. 5 (c). Flow visualization for A = 2 delta wing, α = 25 deg, k = 0.822, R = 0.590.
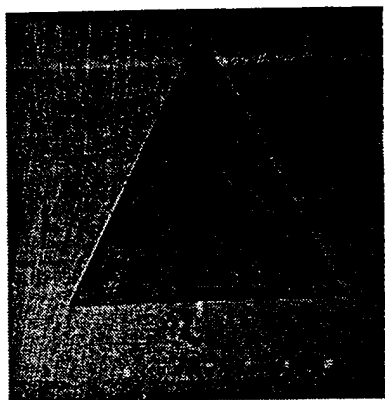
Steady free stream
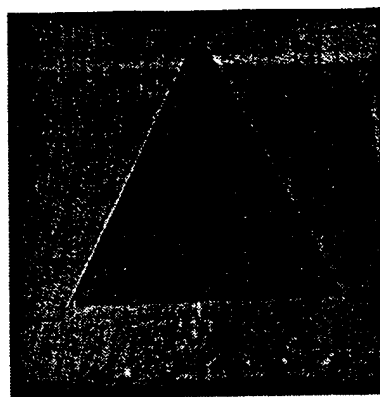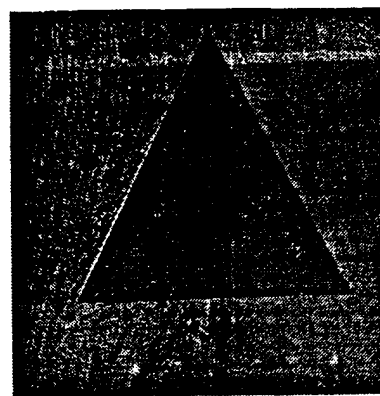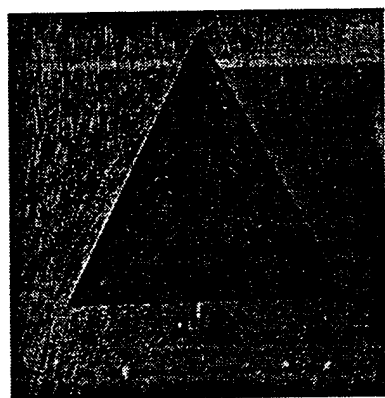
t/T = 0.000
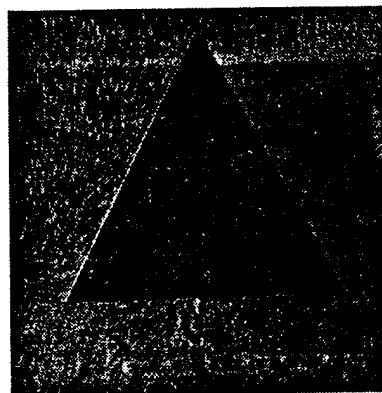
t/T = 0.125
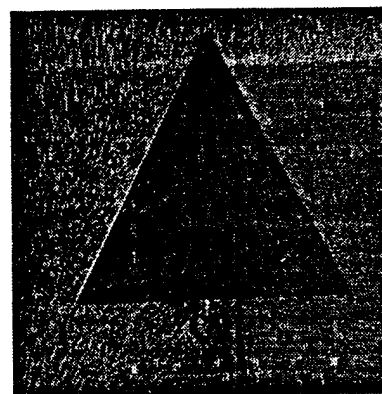
t/T = 0.250
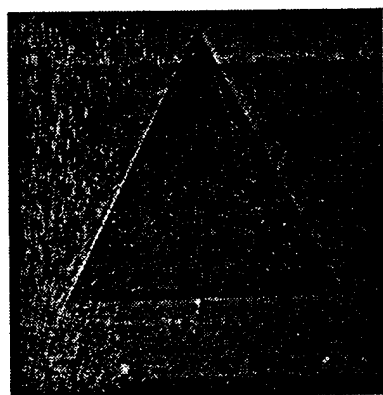
t/T = 0.375
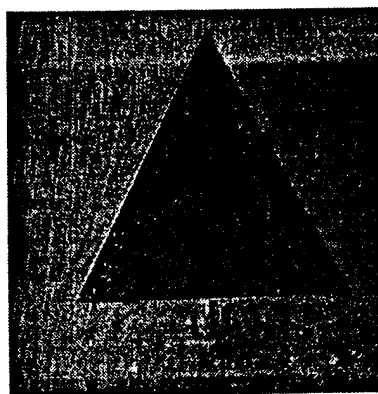
t/T = 0.500
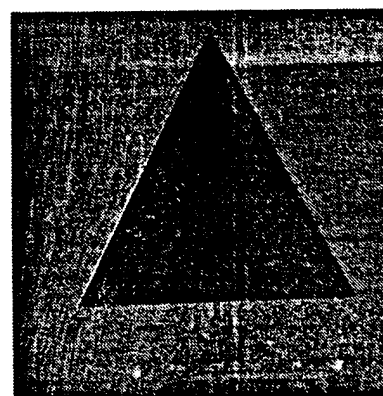
t/T = 0.625

t/T = 0.750

t/T = 0.875

Fig. 5 (d). Flow visualization for A = 2 delta wing, α = 30 deg, k = 0.822, R = 0.589.
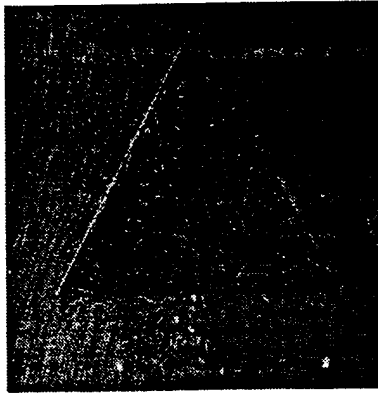
Steady free stream   t/T = 0.000   t/T = 0.125
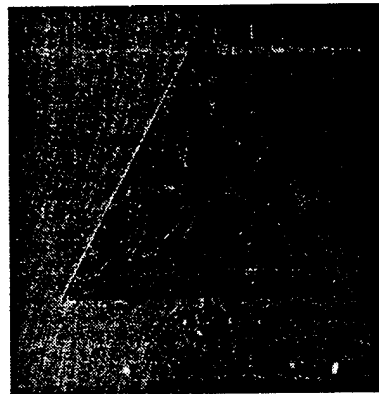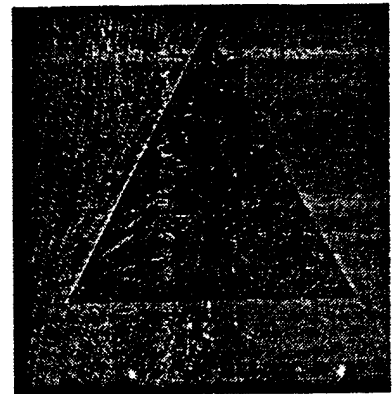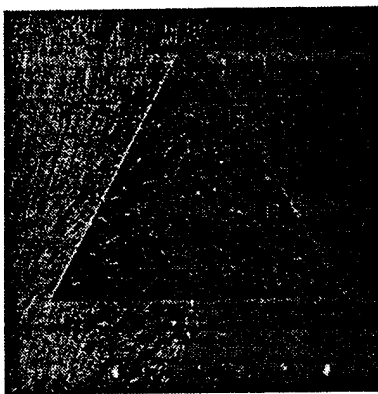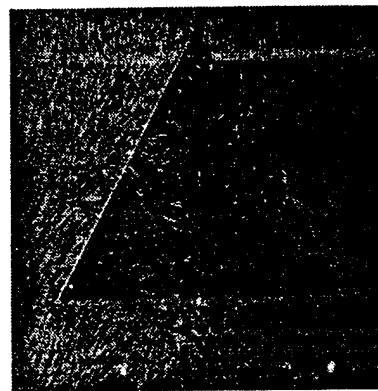
t/T = 0.250   t/T = 0.375   t/T = 0.500
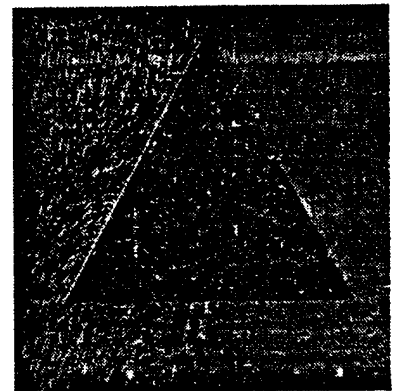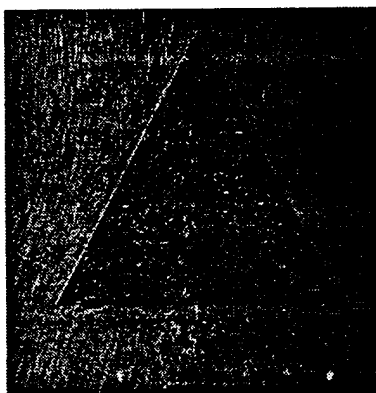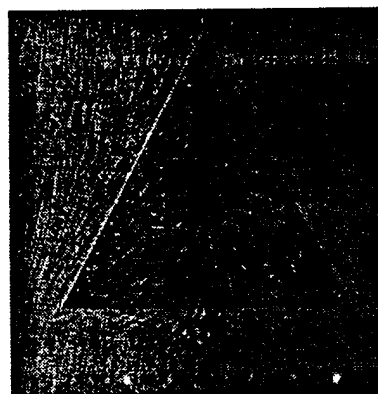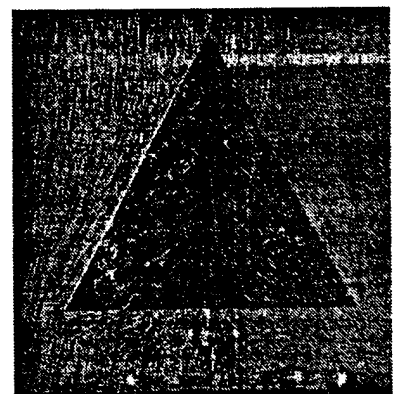
t/T = 0.625   t/T = 0.750   t/T = 0.875

Fig. 5 (e). Flow visualization for A = 2 delta wing, α = 40 deg, k = 0.811, R = 0.581.

t/T = 0.250

X (mm)

Normalized axial velocity $\dfrac{V_x}{U_\infty}$

2.00
1.75
1.50
1.25
1.00
0.75
0.50
0.25
0.00

t/T = 0.000   leading-edge

X (mm)

t/T = 0.375

X (mm)

t/T = 0.125

X (mm)

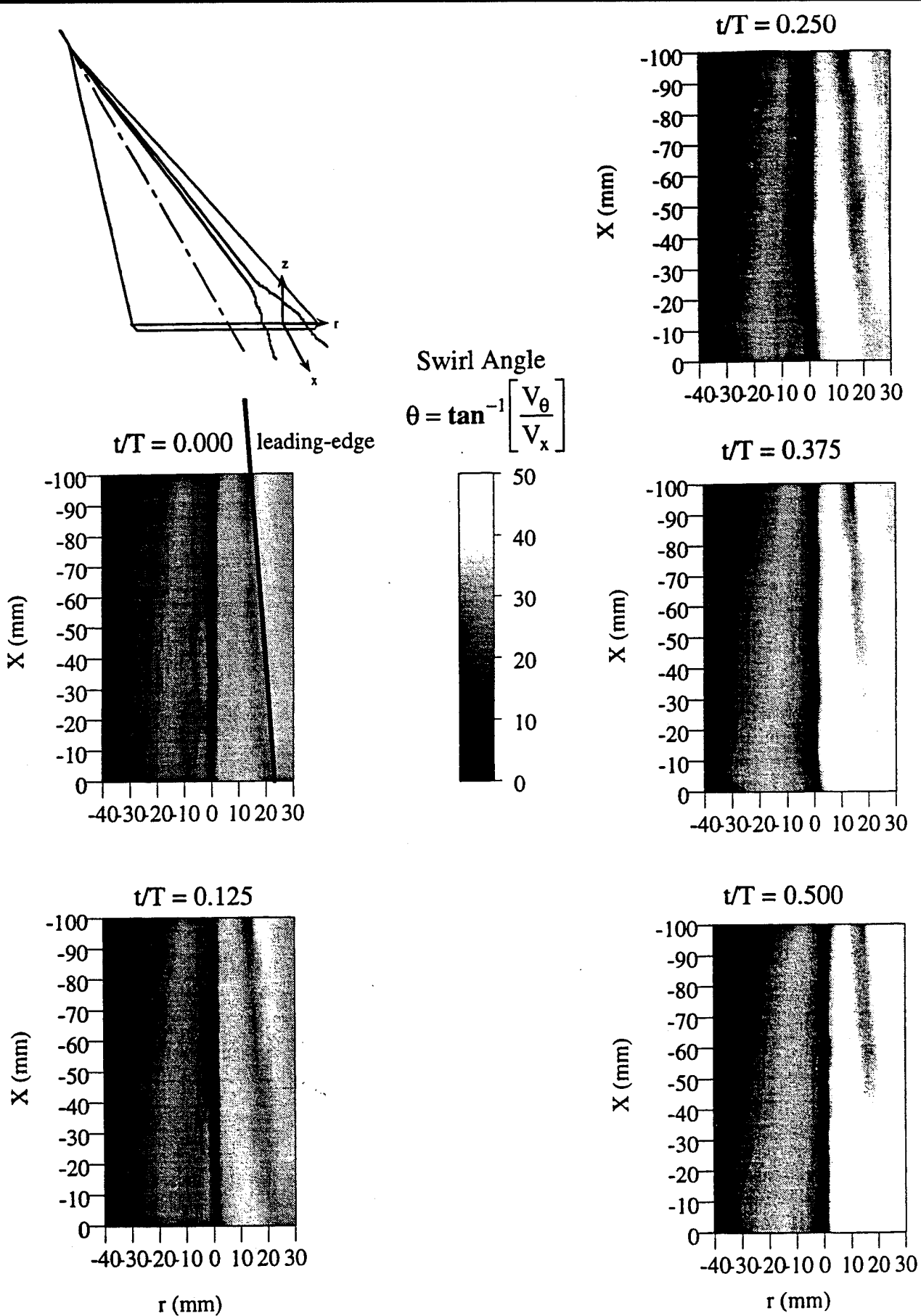t/T = 0.500

X (mm)

r (mm)

r (mm)
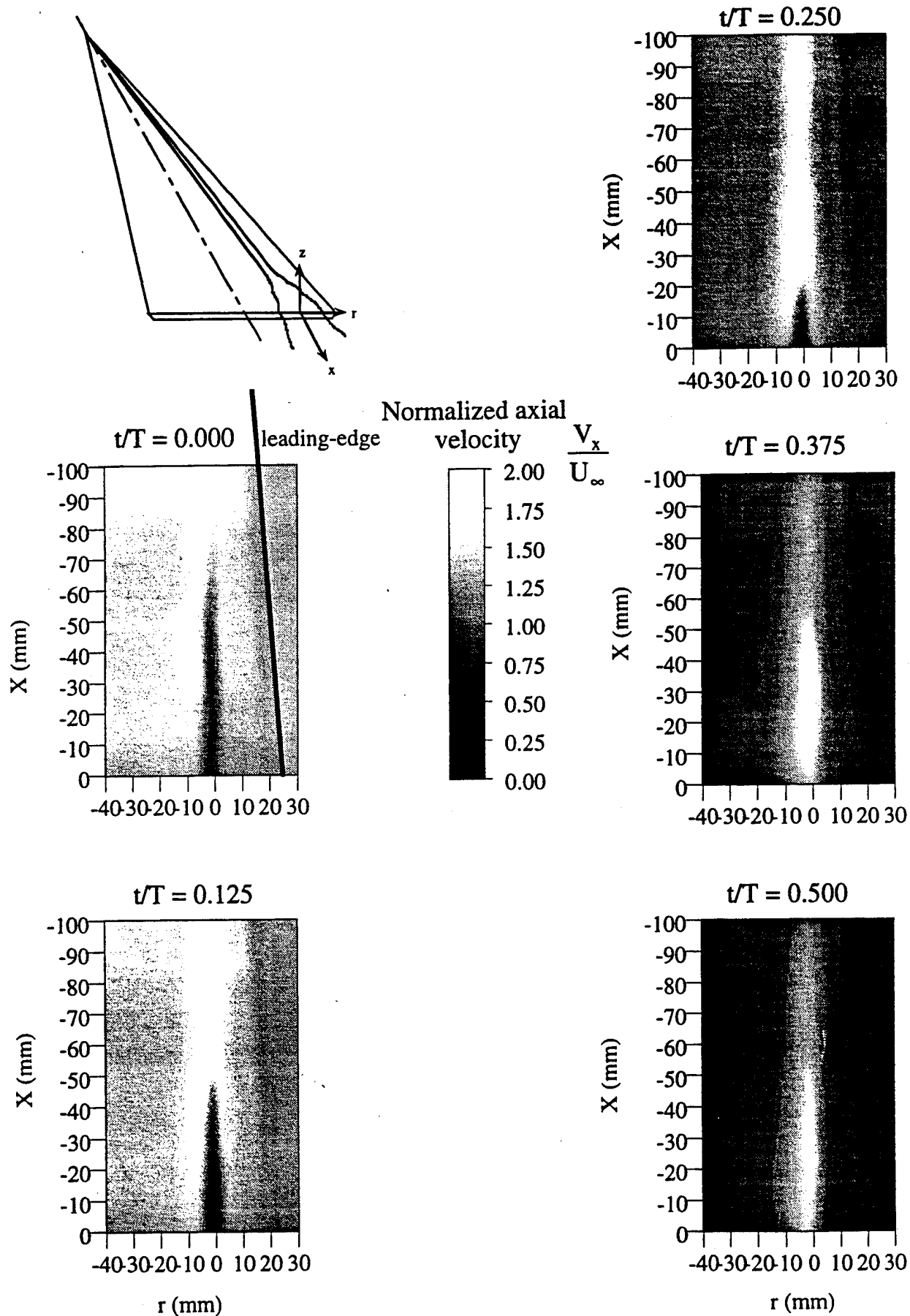
Fig. 6 (a). Normalized axial velocity survey of a plane across the vortex core centerline during flow deceleration. α=15 deg, A = 1, k = 1.27, R = 0.42
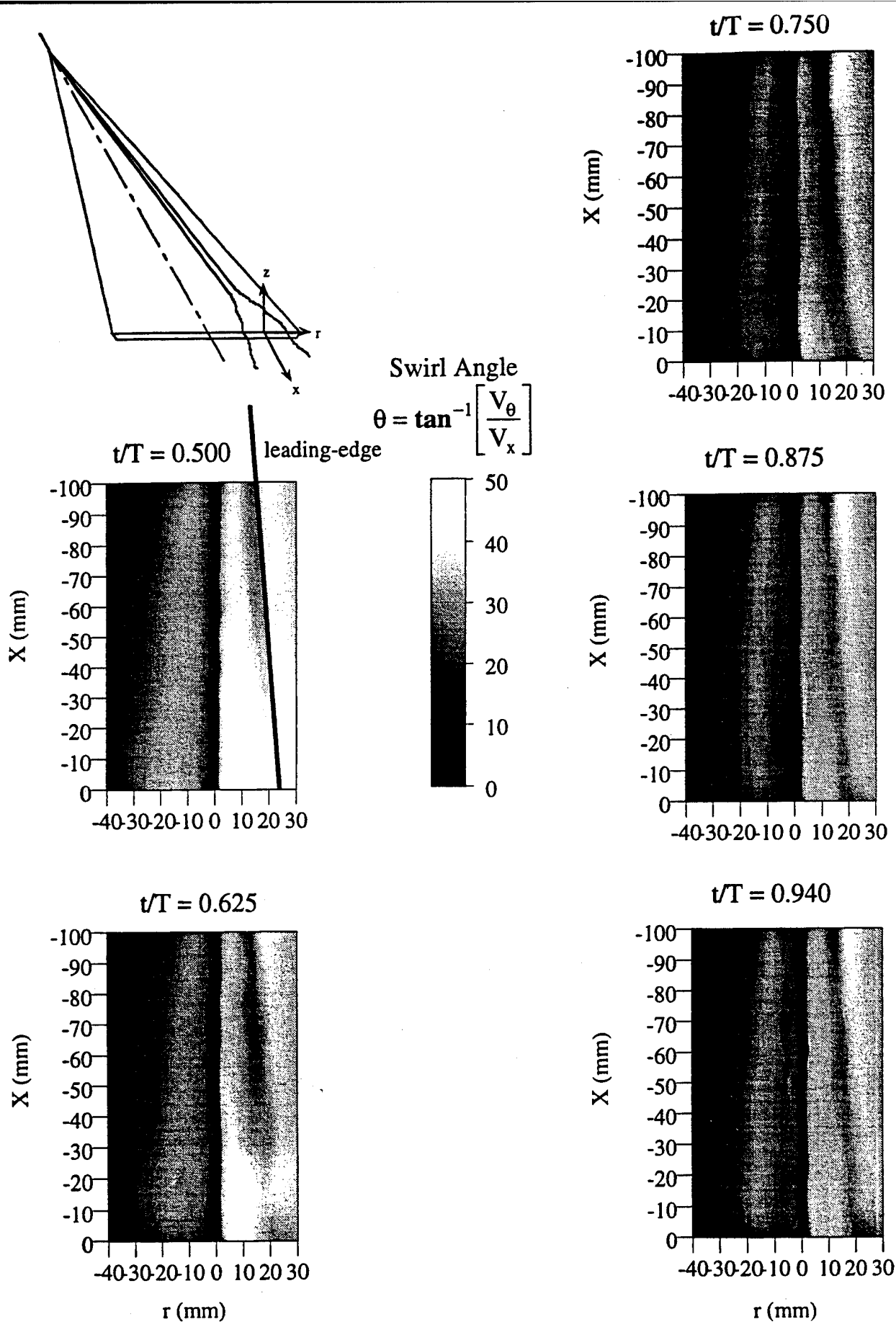
Fig. 6 (b). Normalized axial velocity survey of a plane across the vortex core centerline during flow acceleration. α=15 deg, A = 1, k = 1.27, R = 0.42

t/T = 0.250

Normalized swirl
velocity $\dfrac{V_\theta}{U_\infty}$

t/T = 0.000   leading-edge
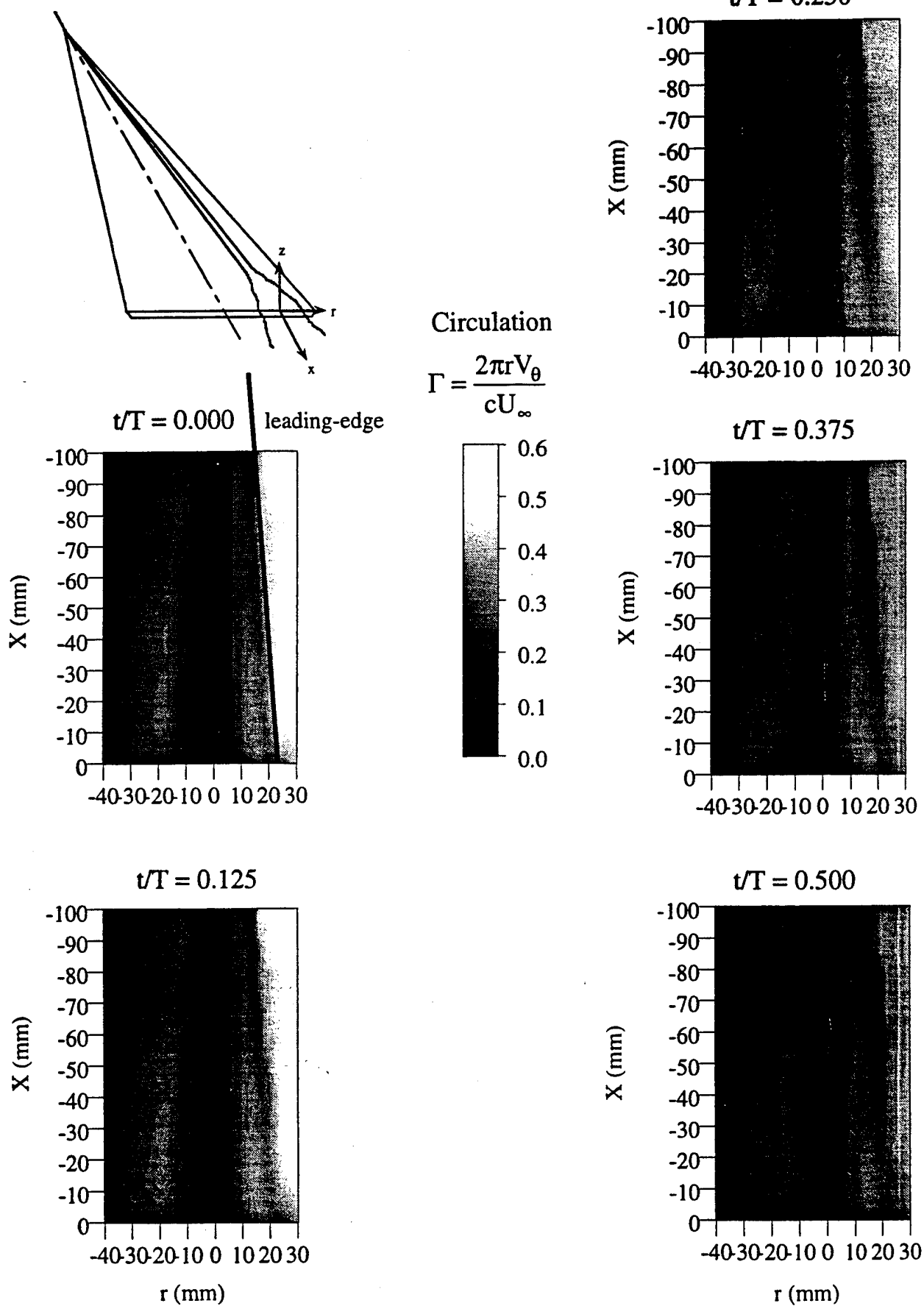
t/T = 0.375

t/T = 0.125

t/T = 0.500

r (mm)

r (mm)

Fig. 7 (a). Normalized swirl velocity survey of a plane across the vortex core
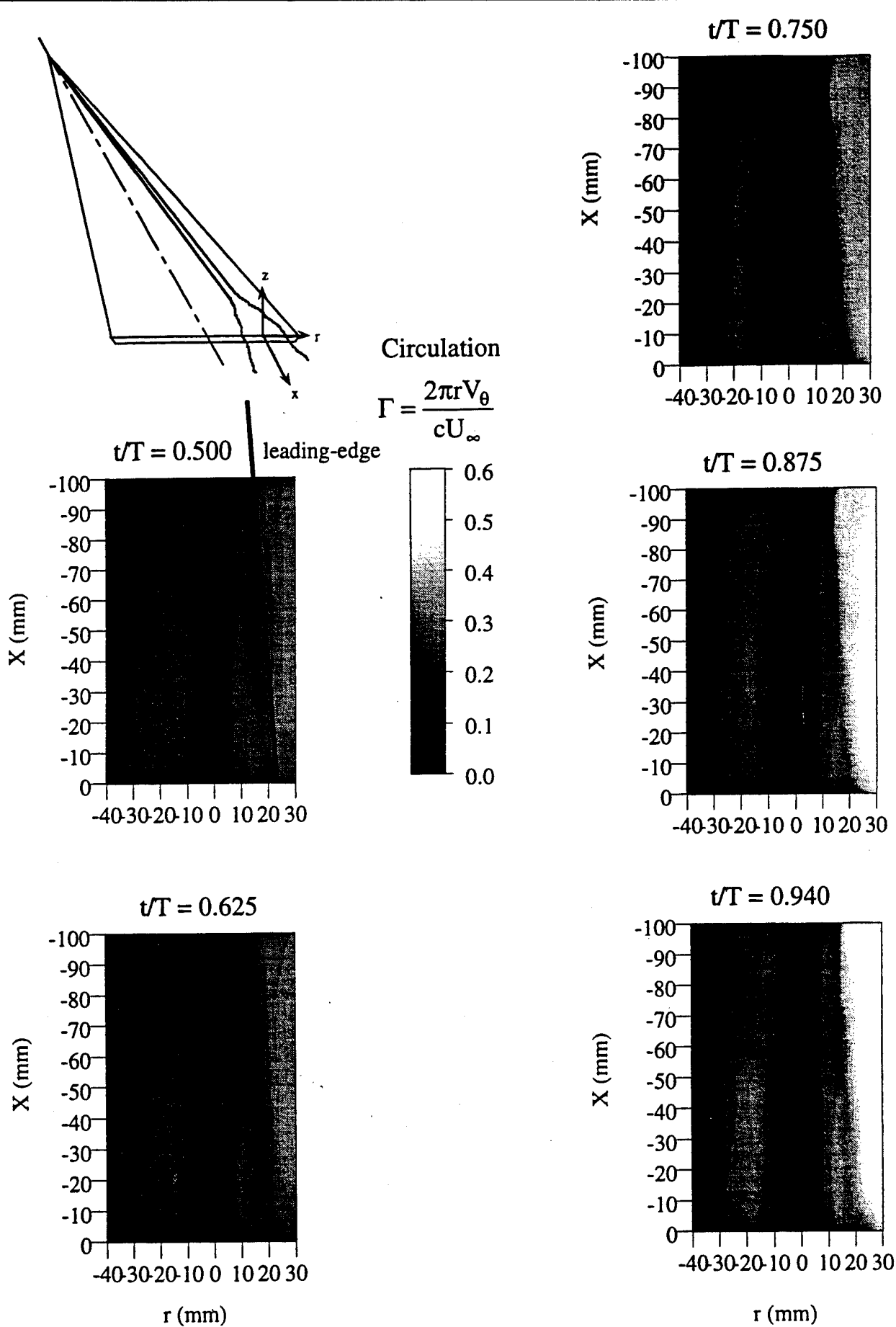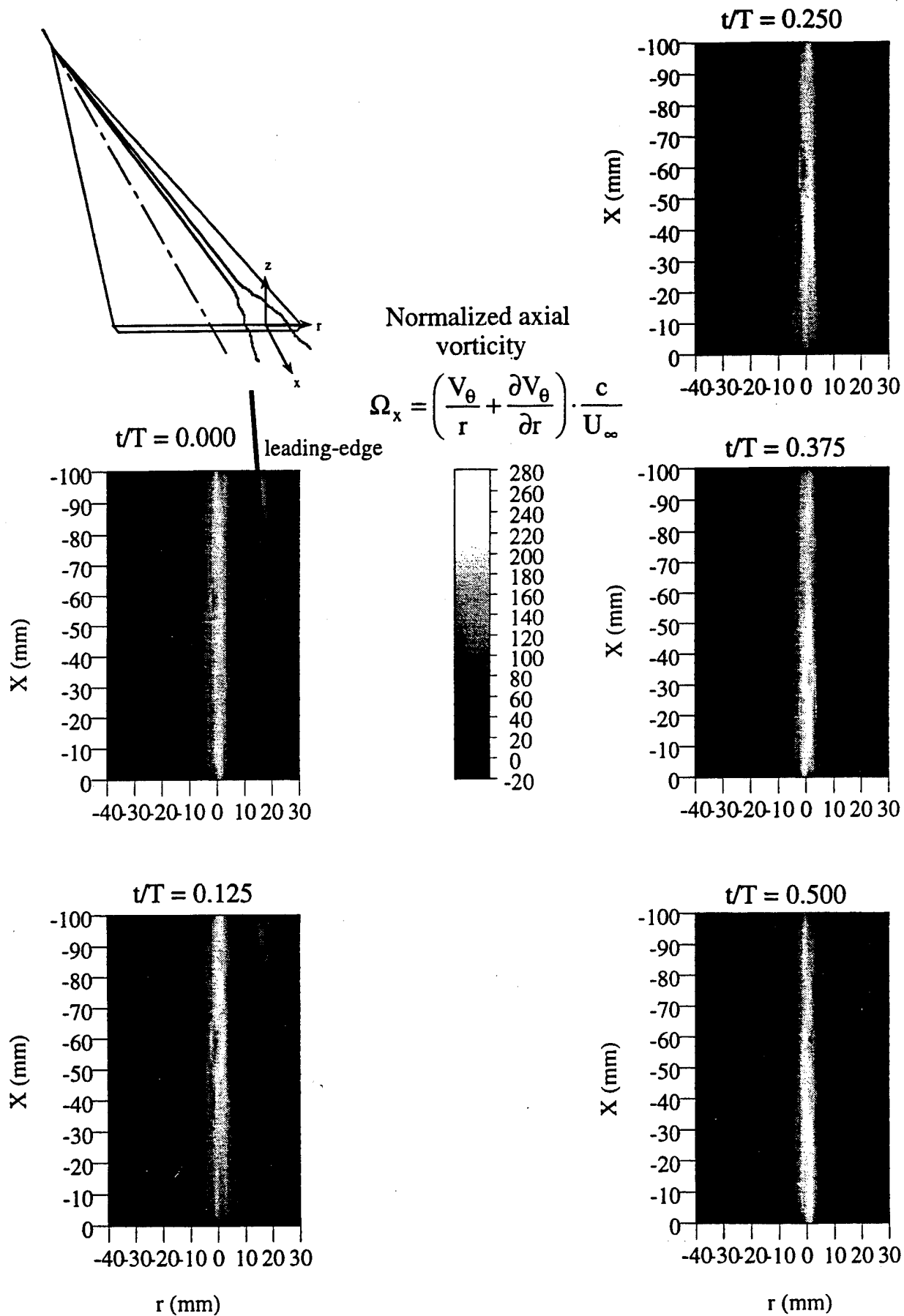centerline during flow deceleration. α=15 deg, A = 1, k = 1.27, R = 0.42

t/T = 0.750
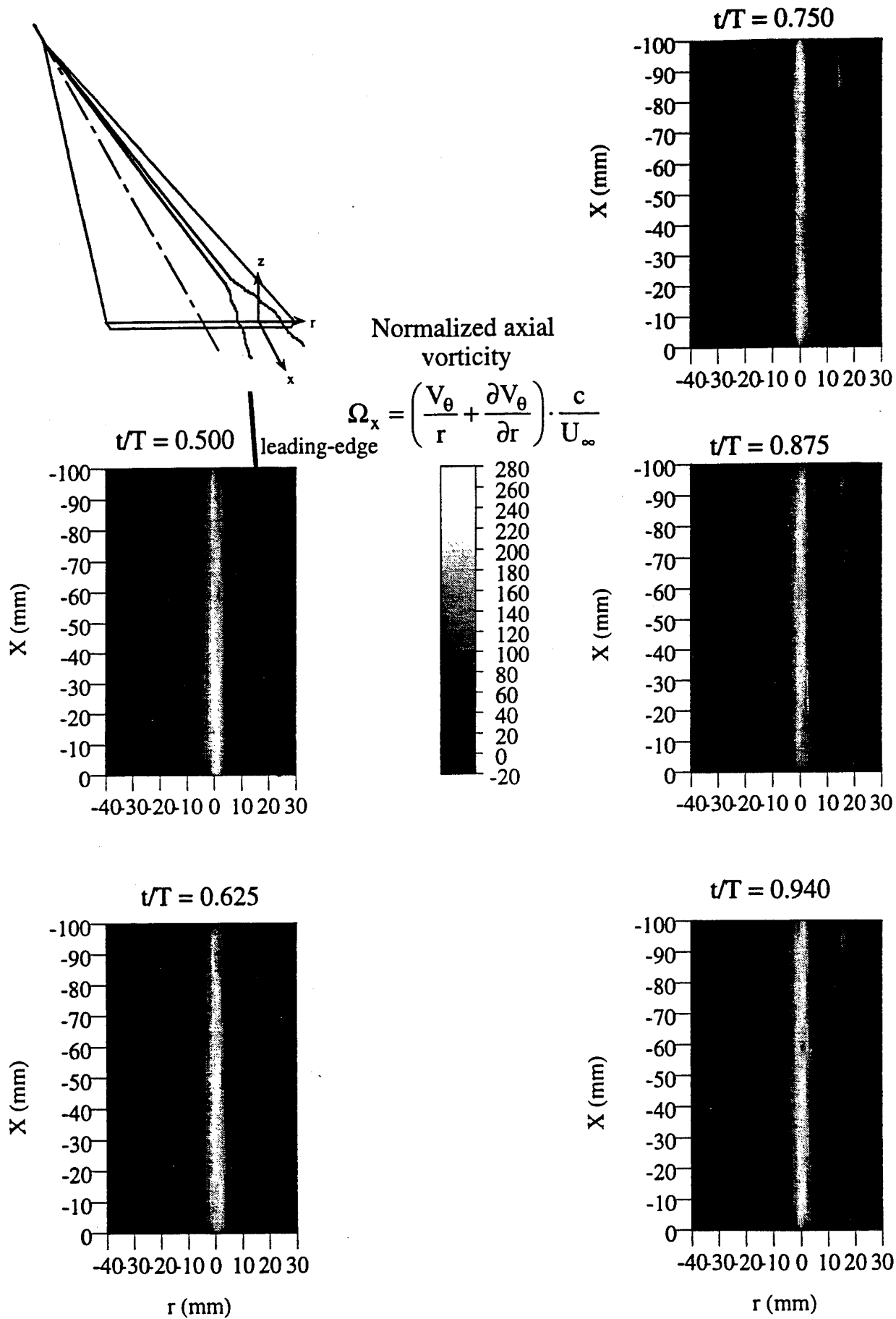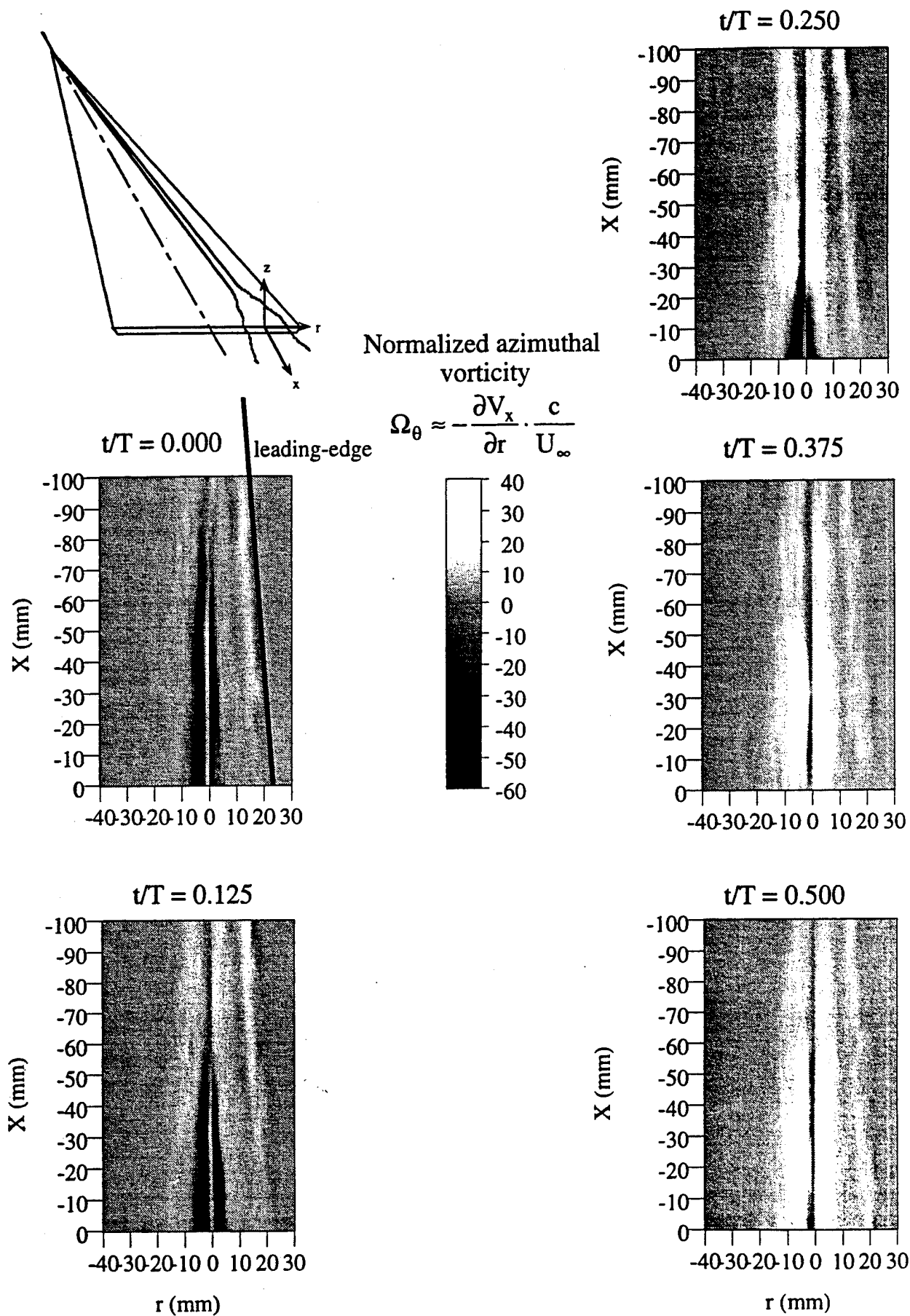
X (mm)

-100 -90 -80 -70 -60 -50 -40 -30 -20 -10 0

-40 -30 -20 -10 0 10 20 30

Normalized swirl
velocity $\dfrac{V_\theta}{U_\infty}$

0.9
0.7
0.5
0.3
0.1
-0.1
-0.3
-0.5
-0.7

t/T = 0.500   leading-edge

X (mm)

-100 -90 -80 -70 -60 -50 -40 -30 -20 -10 0

-40 -30 -20 -10 0 10 20 30

t/T = 0.875

X (mm)

-100 -90 -80 -70 -60 -50 -40 -30 -20 -10 0

-40 -30 -20 -10 0 10 20 30

t/T = 0.625

X (mm)

-100 -90 -80 -70 -60 -50 -40 -30 -20 -10 0

-40 -30 -20 -10 0 10 20 30

r (mm)

t/T = 0.940

X (mm)

-100 -90 -80 -70 -60 -50 -40 -30 -20 -10 0

-40 -30 -20 -10 0 10 20 30

r (mm)
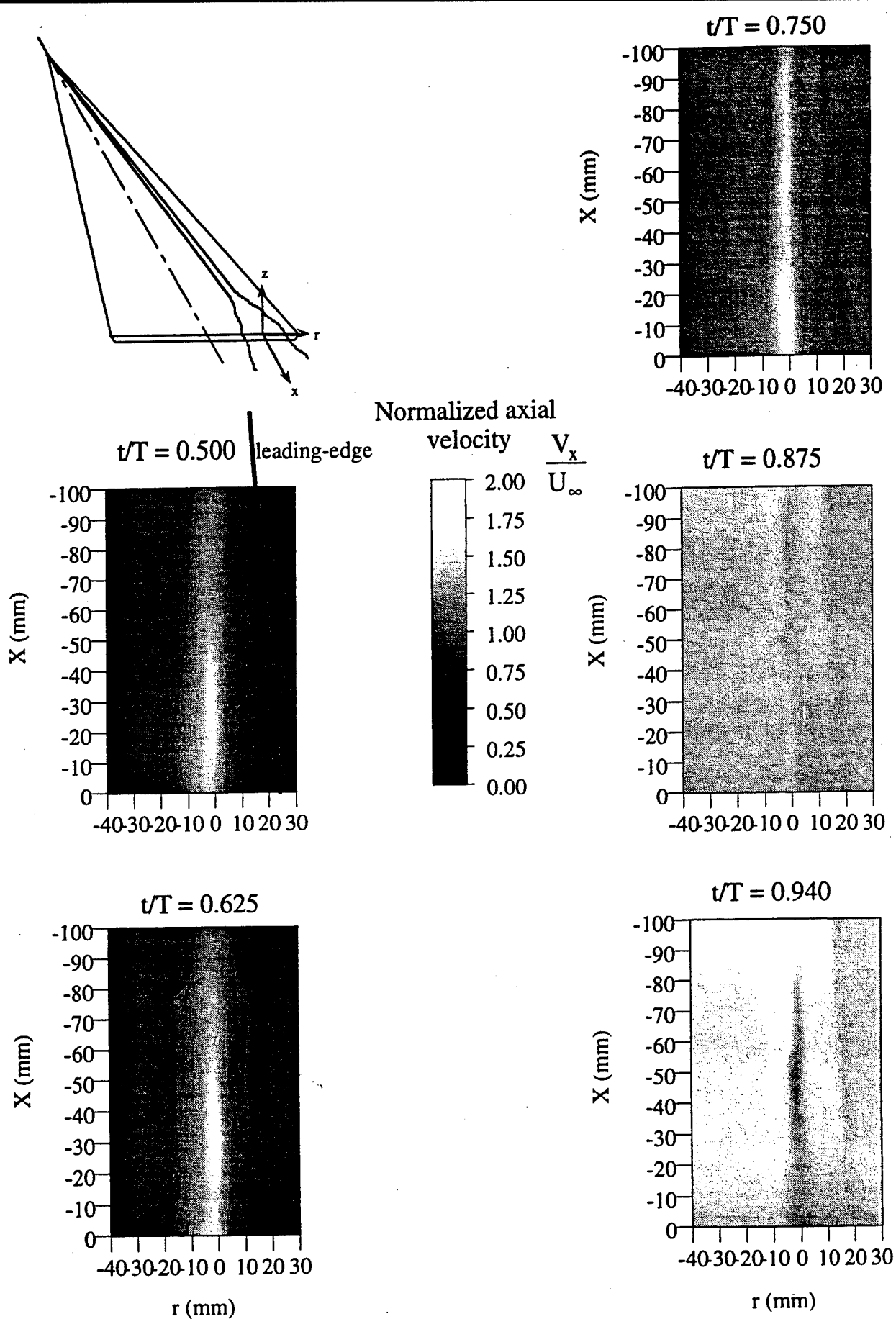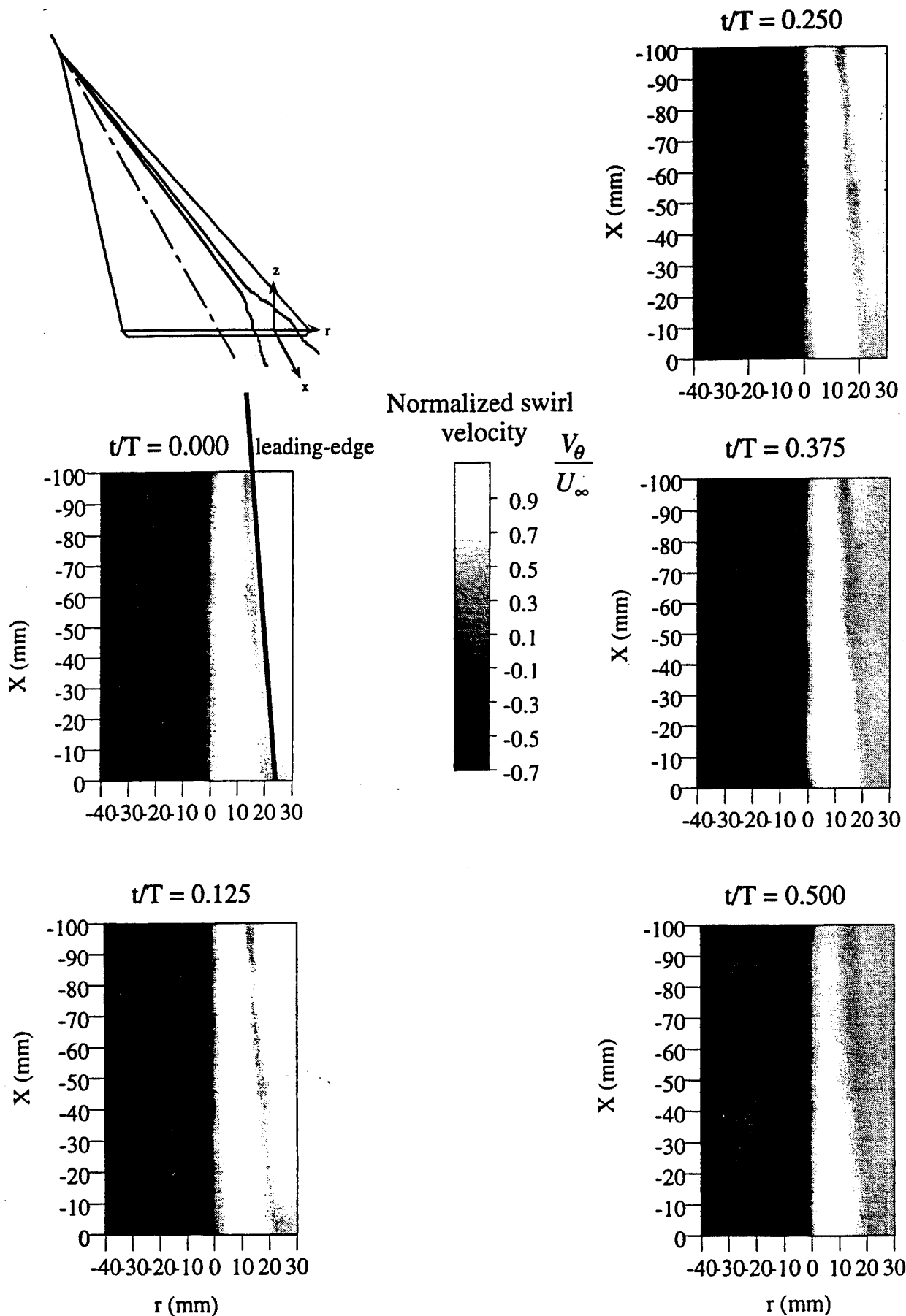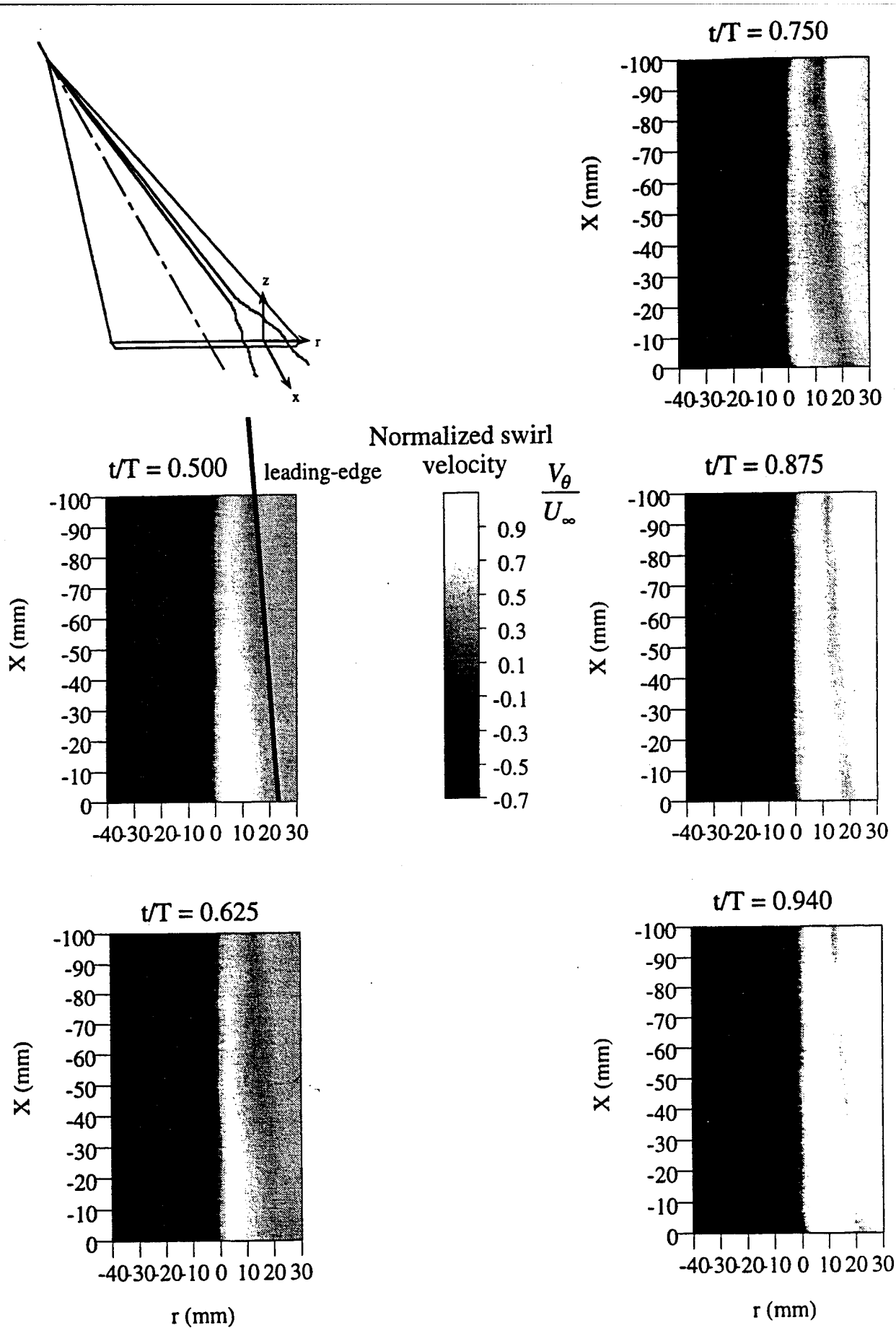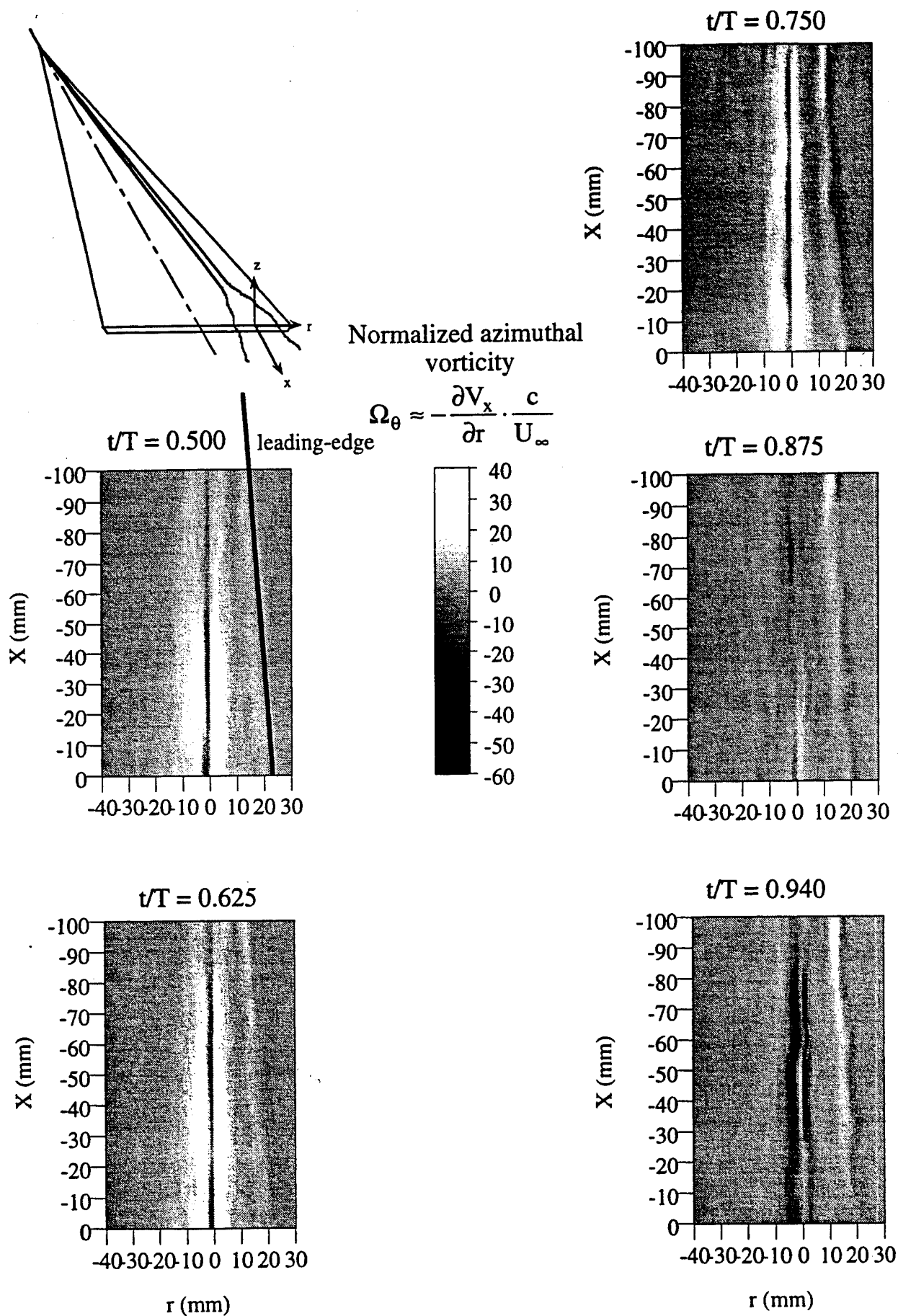
Fig. 7 (b). Normalized swirl velocity survey of a plane across the vortex core centerline during flow acceleration. α=15 deg, A = 1, k = 1.27, R = 0.42

t/T = 0.000

t/T = 0.125

t/T = 0.250
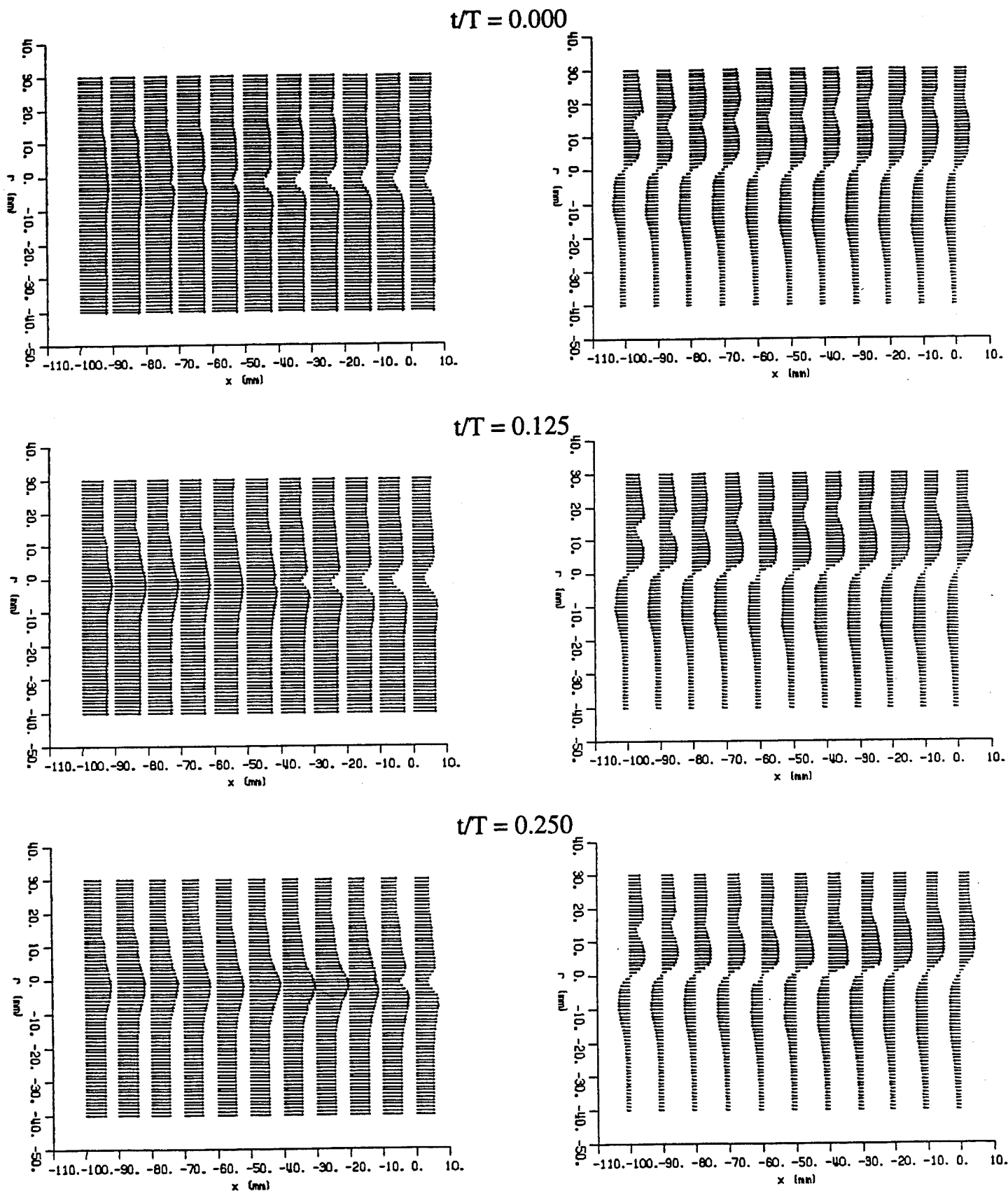
(a) Normalized axial velocity   (b) Normalized swirl velocity
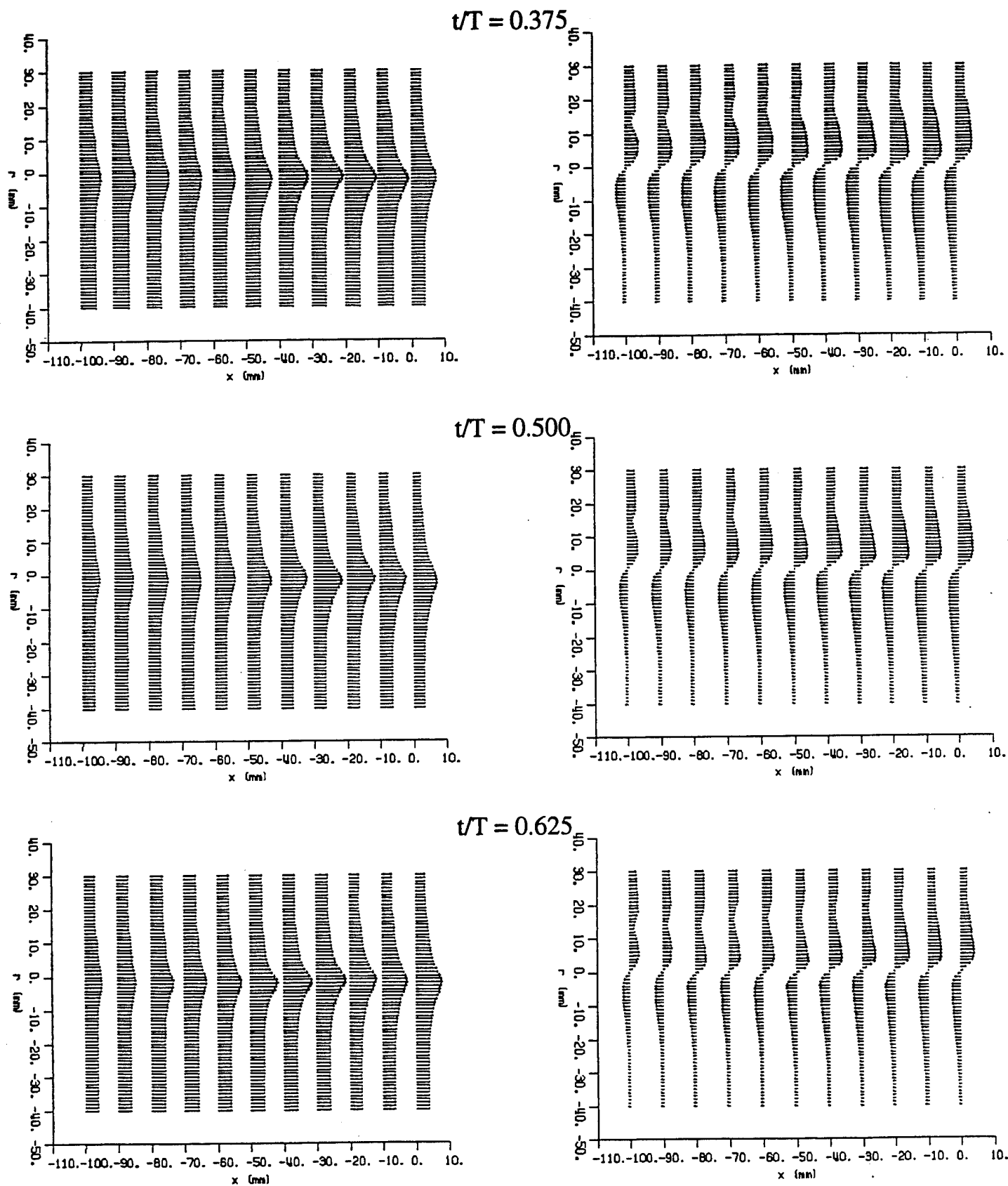
Fig. 8. Velocity vectors in a plane across the vortex core centerline during an unsteady cycle: (a) normalized axial velocity, (b) normalized swirl velociy. α=15 deg., A = 1, k=1.27, R = 0.42.

(a) Normalized axial velocity   (b) Normalized swirl velocity

Fig. 8, Con't. Velocity vectors in a plane across the vortex core centerline during an unsteady cycle: (a) normalized axial velocity, (b) normalized swirl velociy. α=15 deg., A = 1, k=1.27, R = 0.42.

t/T = 0.750

t/T = 0.875

t/T = 0.940
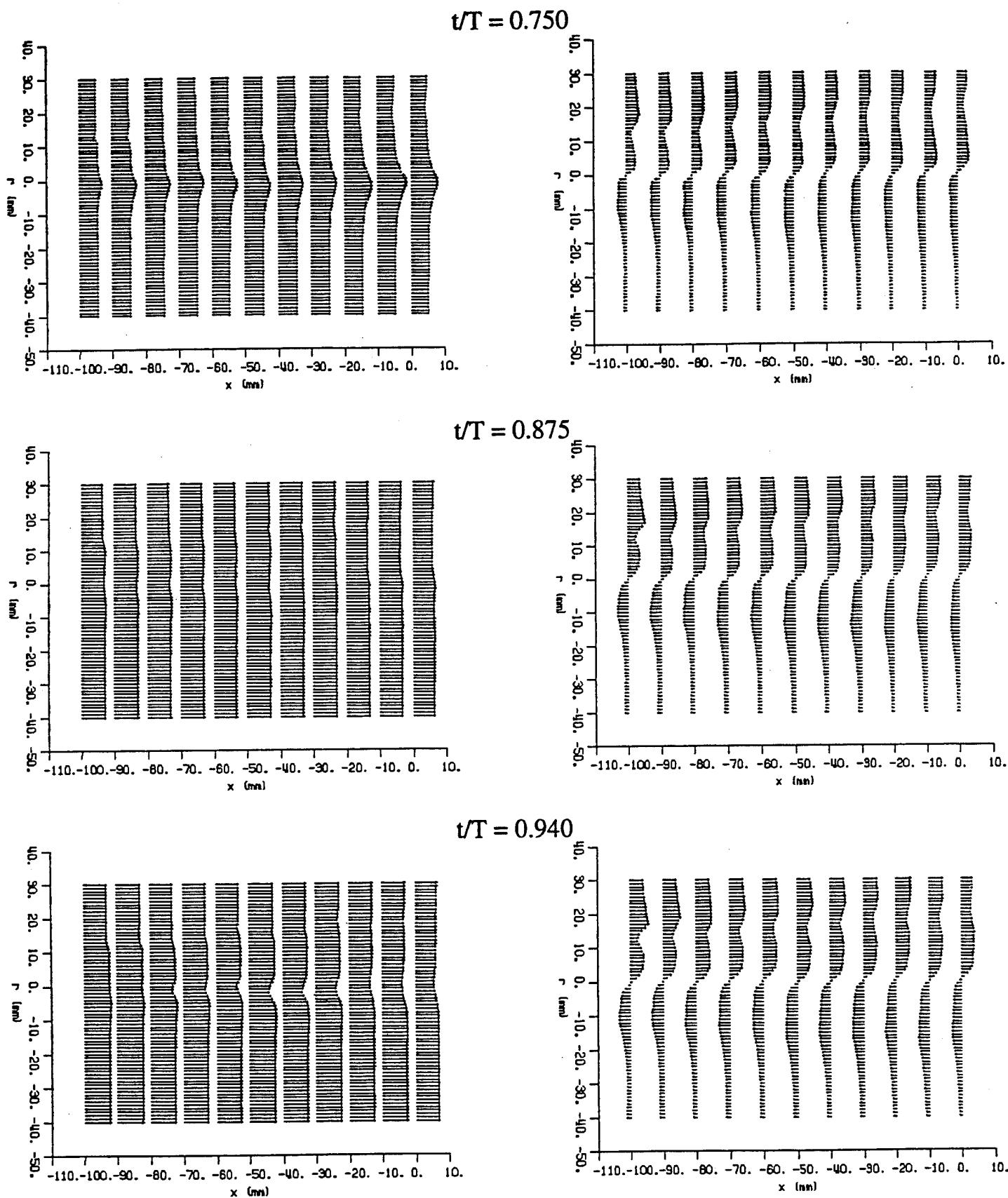
(a) Normalized axial velocity   (b) Normalized swirl velocity

Fig. 8, Con't. Velocity vectors in a plane across the vortex core centerline during an unsteady cycle: (a) normalized axial velocity, (b) normalized swirl velociy. α=15 deg., A = 1, k=1.27, R = 0.42.
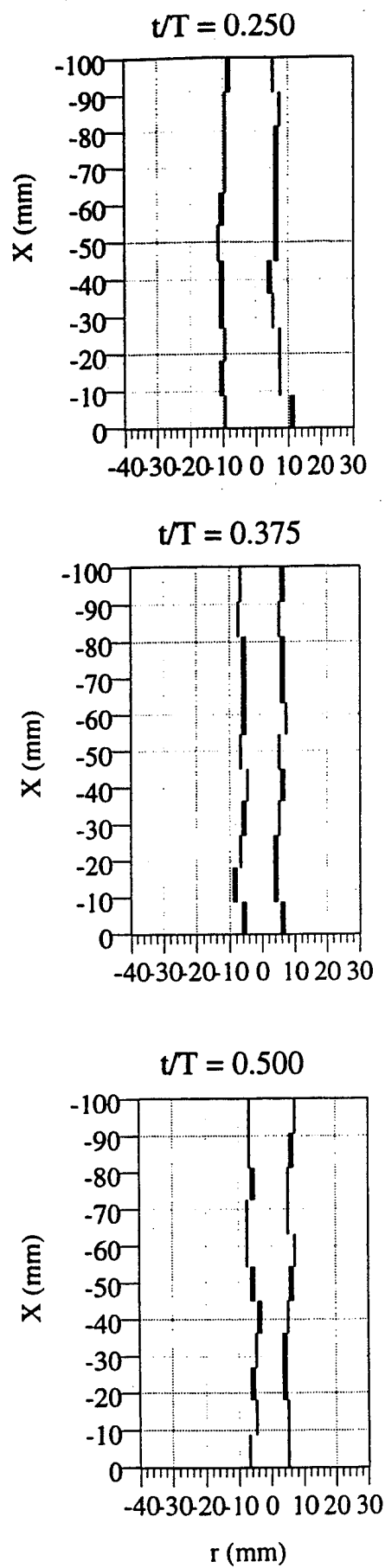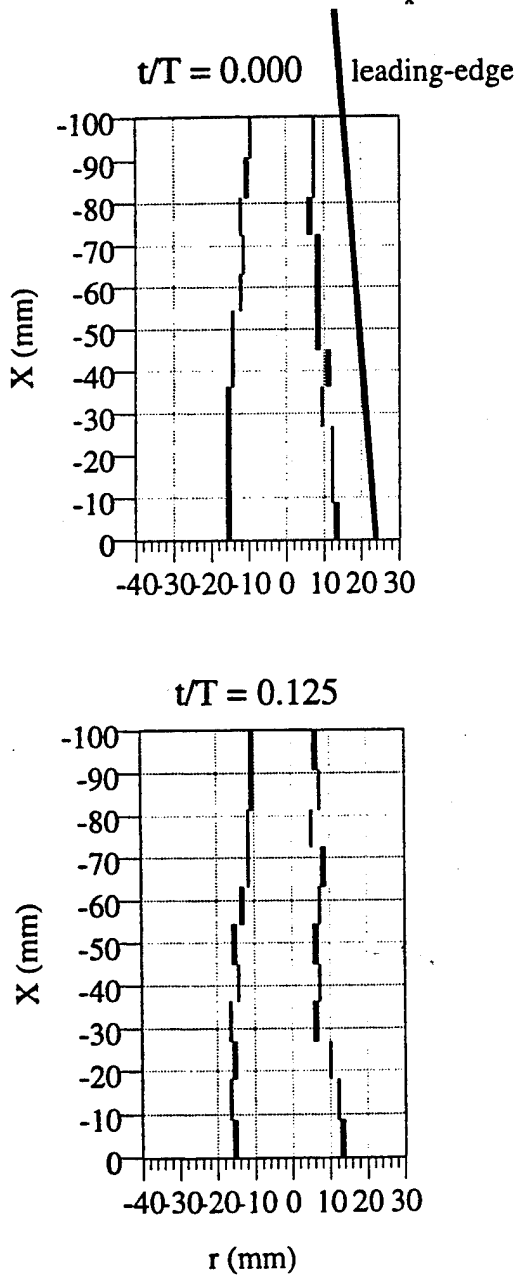
Fig. 9 (a). Variation of vortex viscous core position during deceleration. α=15 deg, A = 1, k = 1.27, R = 0.42
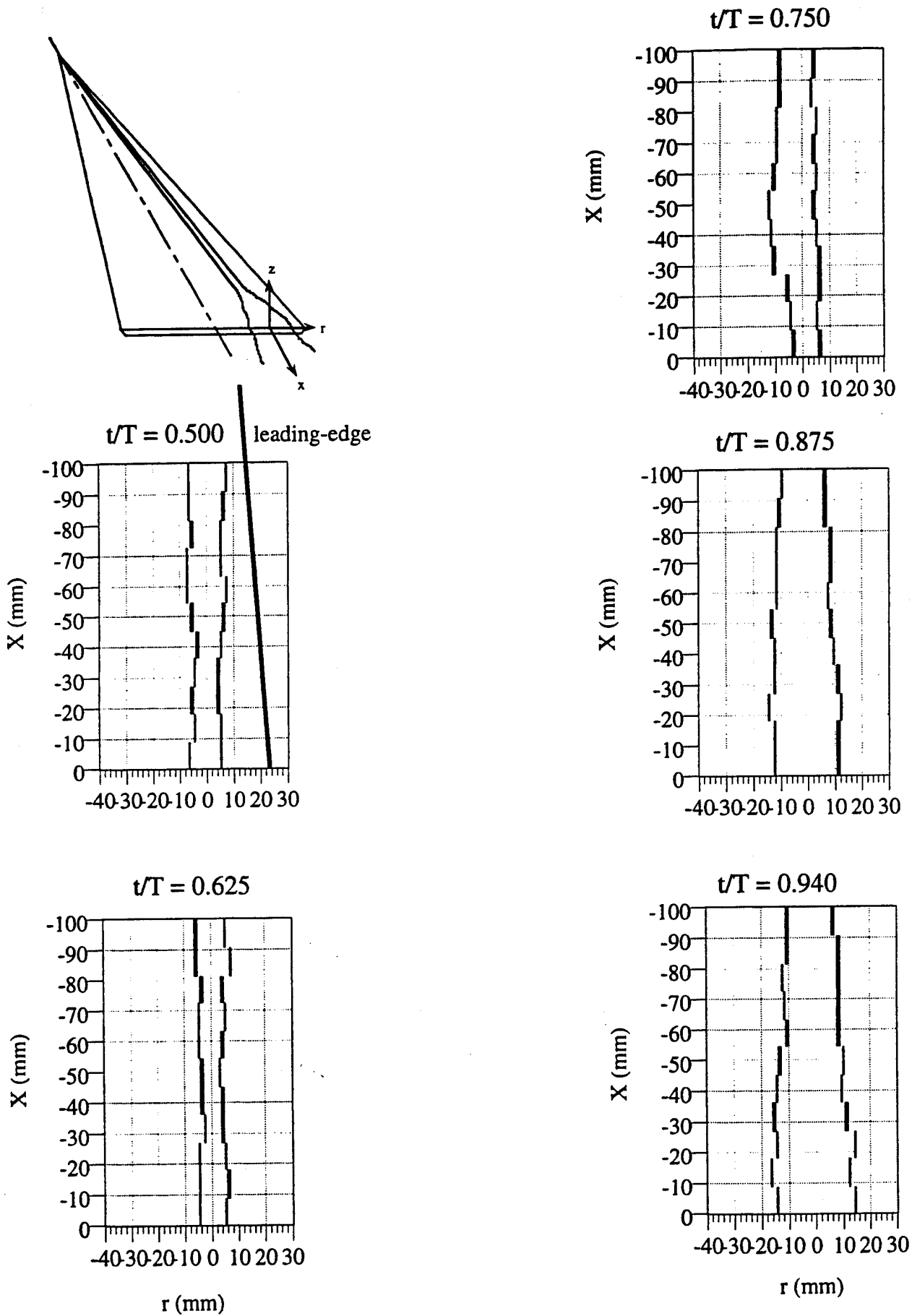
Fig. 9 (b). Variation of vortex viscous core position during acceleration.
α=15 deg, A = 1, k = 1.27, R = 0.42

t/T = 0.250

X (mm)

-100 -90 -80 -70 -60 -50 -40 -30 -20 -10 0

-40 -30 -20 -10 0 10 20 30

Swirl Angle

$$\theta = \tan^{-1}\left[\frac{V_\theta}{V_x}\right]$$

50

40

30

20

10

0

t/T = 0.000   leading-edge

X (mm)

-100 -90 -80 -70 -60 -50 -40 -30 -20 -10 0

-40 -30 -20 -10 0 10 20 30

t/T = 0.375

X (mm)

-100 -90 -80 -70 -60 -50 -40 -30 -20 -10 0

-40 -30 -20 -10 0 10 20 30

t/T = 0.125

X (mm)

-100 -90 -80 -70 -60 -50 -40 -30 -20 -10 0

-40 -30 -20 -10 0 10 20 30

r (mm)

t/T = 0.500

X (mm)

-100 -90 -80 -70 -60 -50 -40 -30 -20 -10 0

-40 -30 -20 -10 0 10 20 30

r (mm)

Fig. 10 (a). Swirl angle survey of a plane across the vortex core centerline during flow deceleration. α=15 deg, A = 1, k = 1.27, R = 0.42

t/T = 0.750

X (mm)

-100 -90 -80 -70 -60 -50 -40 -30 -20 -10 0

-40 -30 -20 -10 0 10 20 30

Swirl Angle

$$\theta = \tan^{-1}\left[\frac{V_\theta}{V_x}\right]$$

leading-edge

t/T = 0.500

X (mm)

-100 -90 -80 -70 -60 -50 -40 -30 -20 -10 0

-40 -30 -20 -10 0 10 20 30

50

40

30

20

10

0

t/T = 0.875

X (mm)

-100 -90 -80 -70 -60 -50 -40 -30 -20 -10 0

-40 -30 -20 -10 0 10 20 30

t/T = 0.625

X (mm)

-100 -90 -80 -70 -60 -50 -40 -30 -20 -10 0

-40 -30 -20 -10 0 10 20 30

r (mm)

t/T = 0.940

X (mm)

-100 -90 -80 -70 -60 -50 -40 -30 -20 -10 0

-40 -30 -20 -10 0 10 20 30

r (mm)

Fig. 10 (b). Swirl angle survey of a plane across the vortex core centerline during flow acceleration. α=15 deg, A = 1, k = 1.27, R = 0.42

t/T = 0.250

Circulation

$$\Gamma = \frac{2\pi r V_\theta}{c U_\infty}$$

t/T = 0.000 leading-edge

t/T = 0.375

t/T = 0.125

t/T = 0.500

r (mm)

r (mm)

Fig. 11 (a). Normalized circulation survey of a plane across the vortex core centerline during flow deceleration. α=15 deg, A = 1, k = 1.27, R = 0.42

t/T = 0.750

t/T = 0.500

leading-edge

Circulation

$$\Gamma = \frac{2\pi r V_\theta}{c U_\infty}$$

t/T = 0.875

t/T = 0.625

t/T = 0.940

r (mm)

r (mm)

Fig. 11 (b). Normalized circulation survey of a plane across the vortex core centerline during flow acceleration. α=15 deg, A = 1, k = 1.27, R = 0.42

t/T = 0.250

X (mm)

-40-30-20-10 0 10 20 30

Normalized axial vorticity

$$\Omega_x = \left(\frac{V_\theta}{r} + \frac{\partial V_\theta}{\partial r} \right) \cdot \frac{c}{U_\infty}$$

leading-edge

t/T = 0.000

X (mm)

-40-30-20-10 0 10 20 30

280
260
240
220
200
180
160
140
120
100
80
60
40
20
0
-20

t/T = 0.375

X (mm)

-40-30-20-10 0 10 20 30

t/T = 0.125

X (mm)

-40-30-20-10 0 10 20 30

r (mm)

t/T = 0.500

X (mm)

-40-30-20-10 0 10 20 30

r (mm)

Fig. 12 (a). Normalized axial vorticity survey of a plane across the vortex core centerline during flow deceleration. α=15 deg, A = 1, k = 1.27, R = 0.42

t/T = 0.750

t/T = 0.500

Normalized axial vorticity

$$\Omega_x = \left(\frac{V_\theta}{r} + \frac{\partial V_\theta}{\partial r} \right) \cdot \frac{c}{U_\infty}$$

leading-edge

t/T = 0.875

t/T = 0.625

t/T = 0.940

Fig. 12 (b). Normalized axial vorticity survey of a plane across the vortex core centerline during flow acceleration. α=15 deg, A = 1, k = 1.27, R = 0.42

t/T = 0.250

t/T = 0.000

Normalized azimuthal vorticity

$$\Omega_\theta \approx -\frac{\partial V_x}{\partial r} \cdot \frac{c}{U_\infty}$$

leading-edge

t/T = 0.375

t/T = 0.125

t/T = 0.500

r (mm)

r (mm)

Fig. 13 (a). Normalized azimuthal vorticity survey of a plane across the vortex core centerline during flow deceleration. α=15 deg, A = 1, k = 1.27, R = 0.42

t/T = 0.750

t/T = 0.500

Normalized azimuthal
vorticity

$$\Omega_\theta \approx -\frac{\partial V_x}{\partial r} \cdot \frac{c}{U_\infty}$$

leading-edge

t/T = 0.875

t/T = 0.625

t/T = 0.940

r (mm)

r (mm)

Fig. 13 (b). Normalized azimuthal vorticity survey of a plane across the vortex core centerline during flow acceleration. α=15 deg, A = 1, k = 1.27, R = 0.42
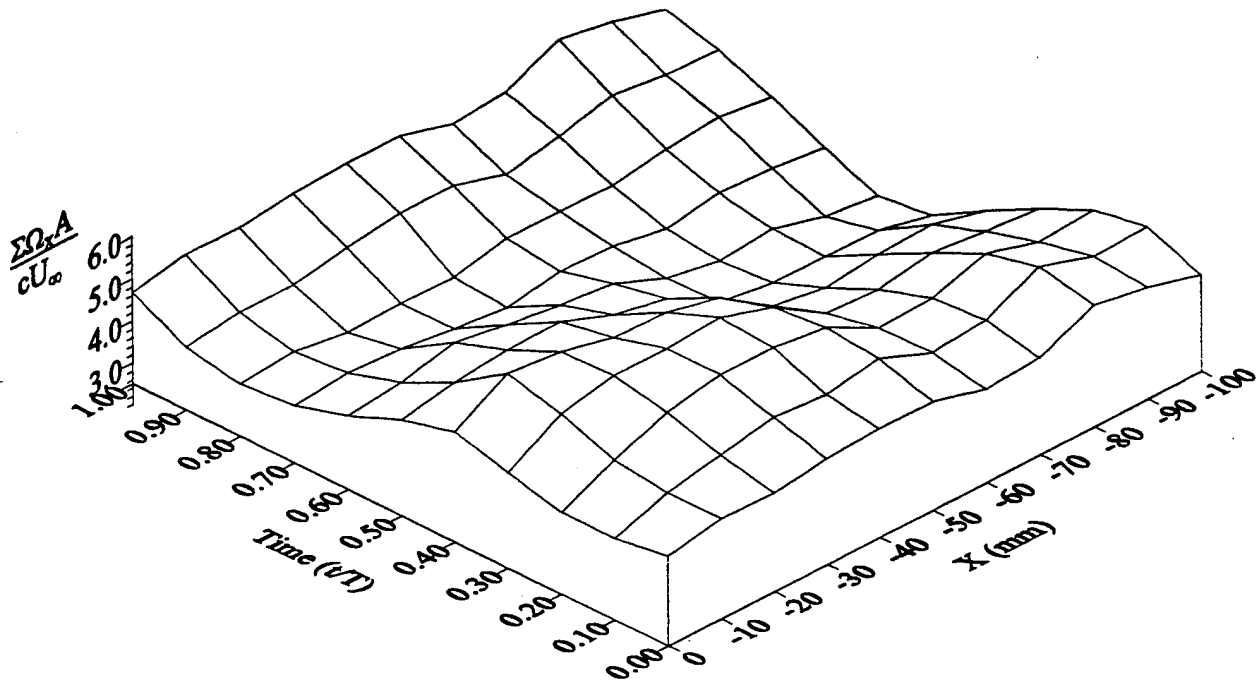
(a) Integrated axial vorticity
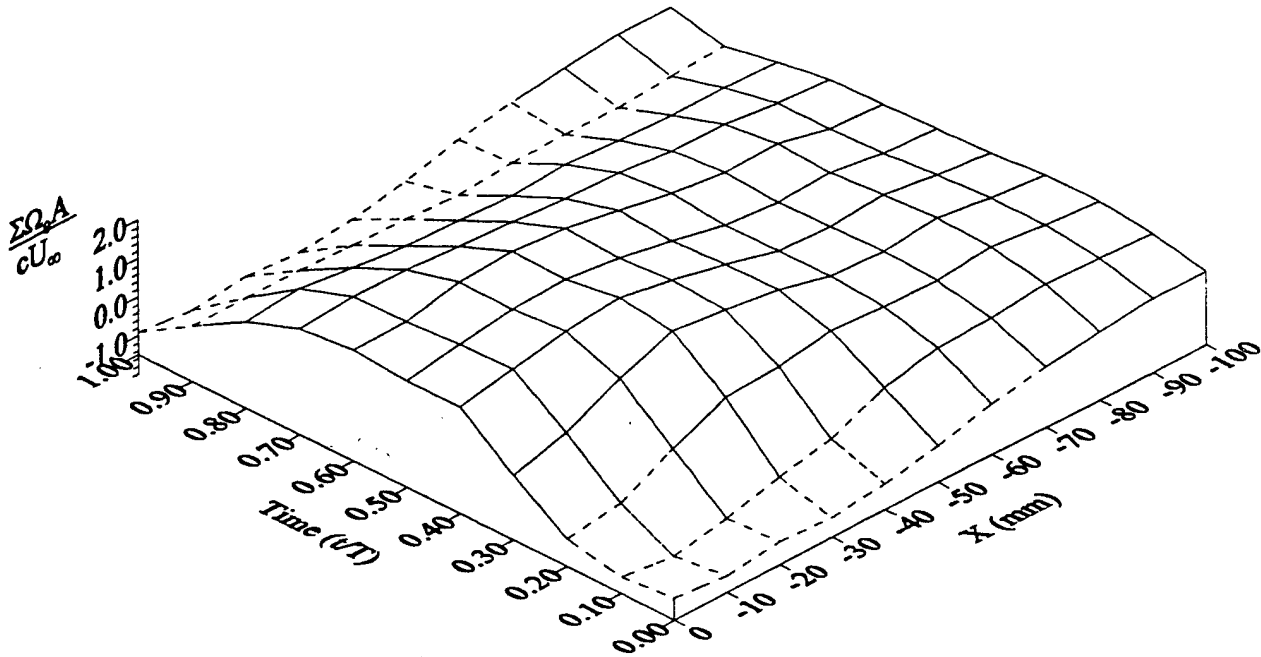
(b) Integrated azimuthal vorticity

Fig. 14. Temporal variation of integrated vorticity values at different streamwise locations. $\alpha = 15$ deg, $A = 1$, $k = 1.27$, $R = 0.42$.
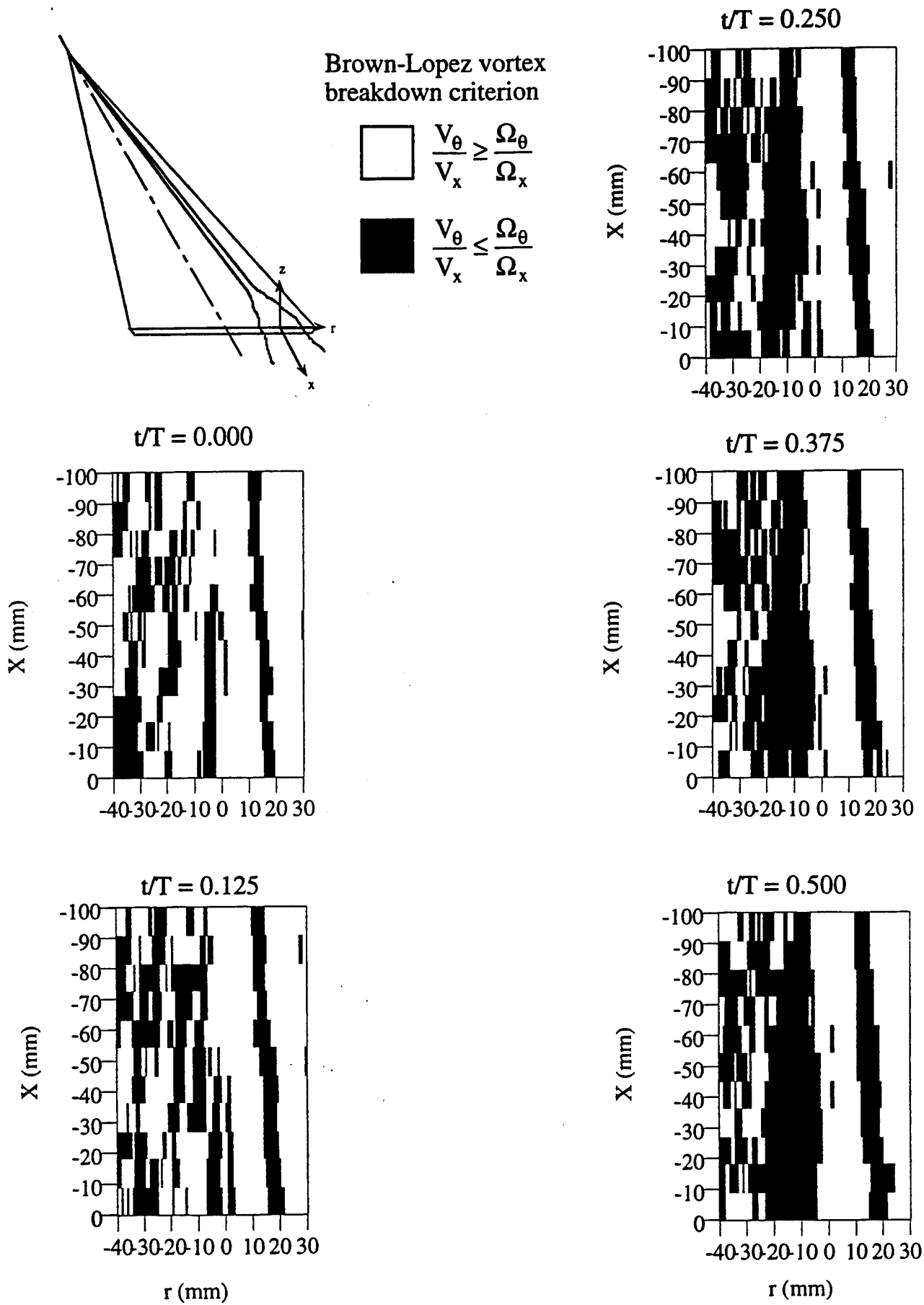
Fig. 15 (a). Brown and Lopez vortex breakdown criterion across the vortex centerline during deceleration. $\alpha=15$ deg, A = 1, k = 1.27, R = 0.42

t/T = 0.750

Brown-Lopez vortex
breakdown criterion

$$\frac{V_\theta}{V_x} \geq \frac{\Omega_\theta}{\Omega_x}$$

$$\frac{V_\theta}{V_x} \leq \frac{\Omega_\theta}{\Omega_x}$$

X (mm)

r (mm)

t/T = 0.500

X (mm)

t/T = 0.875

X (mm)

t/T = 0.625

X (mm)

r (mm)

t/T = 0.940

X (mm)

r (mm)
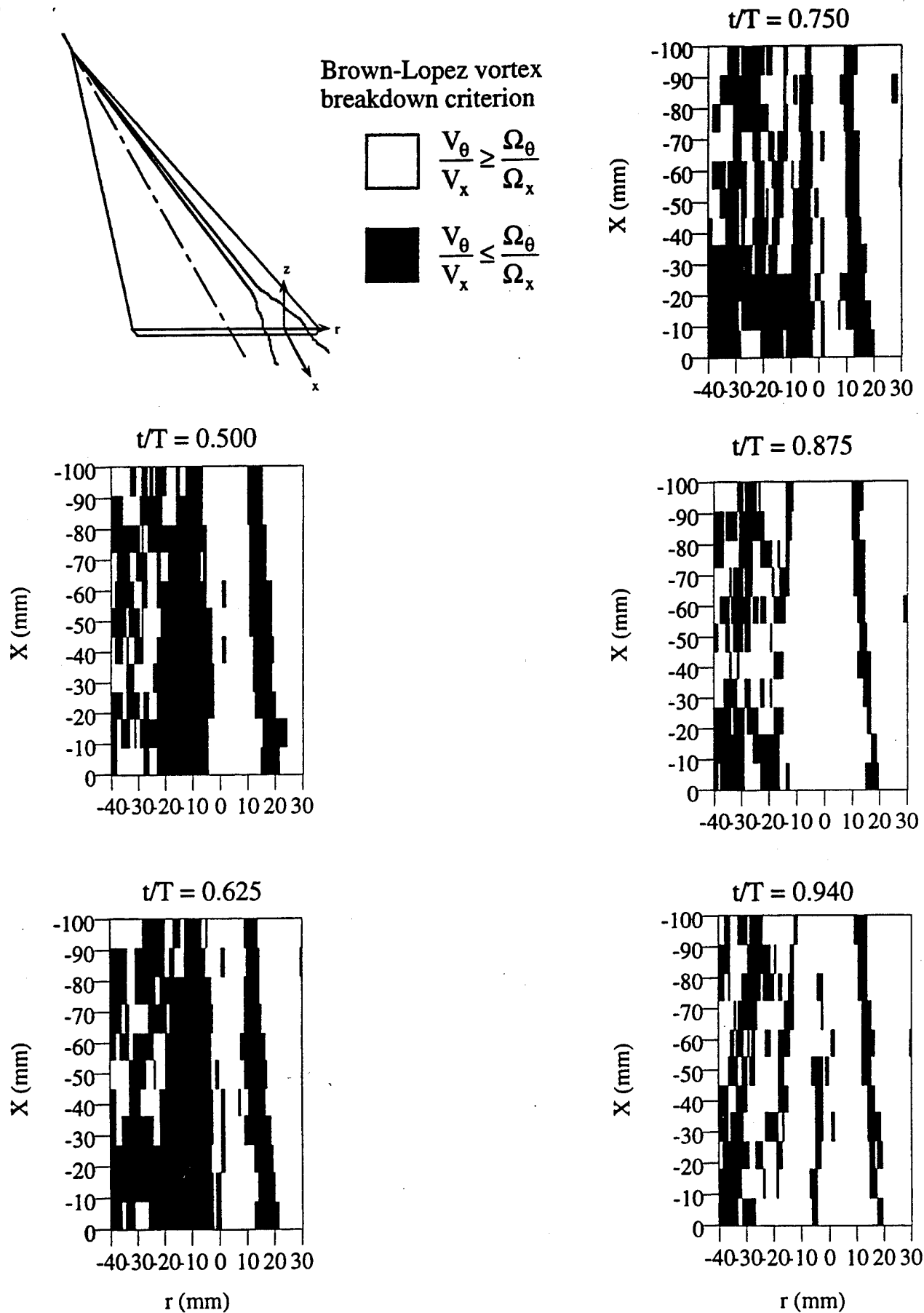
Fig. 15 (b). Brown and Lopez vortex breakdown criterion across the vortex
centerline during deceleration. α=15 deg, A = 1, k = 1.27, R = 0.42

t/T = 0.000

t/T = 0.125

t/T = 0.250

t/T = 0.375

t/T = 0.500
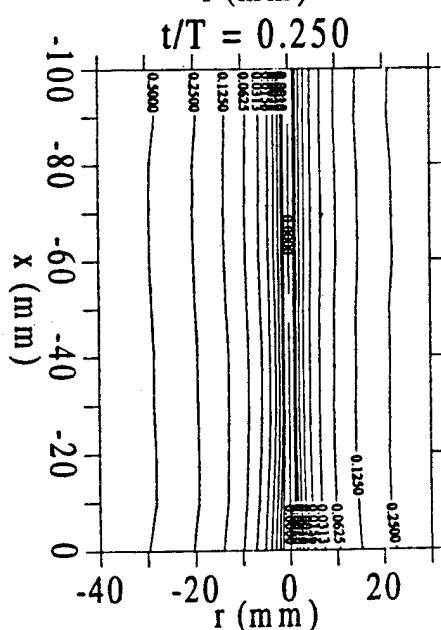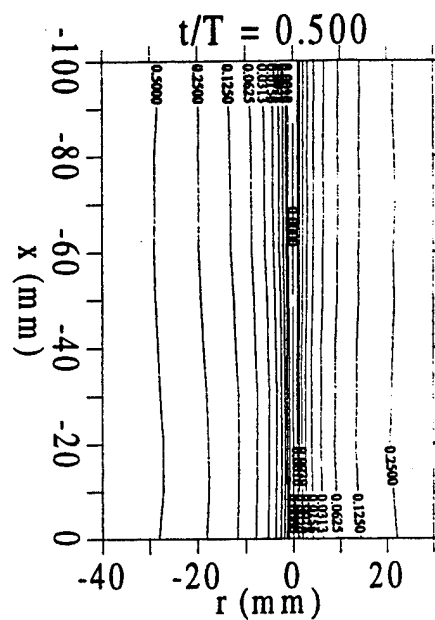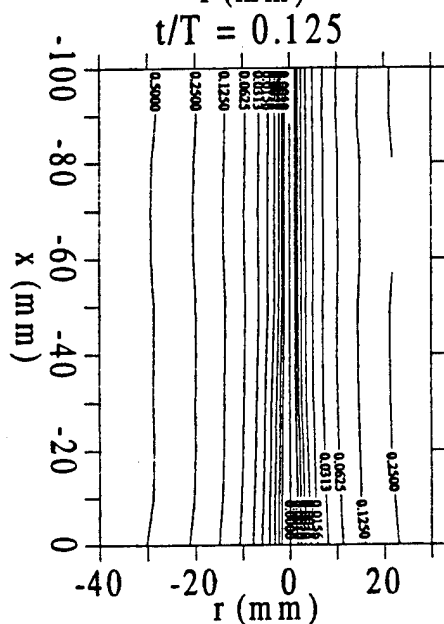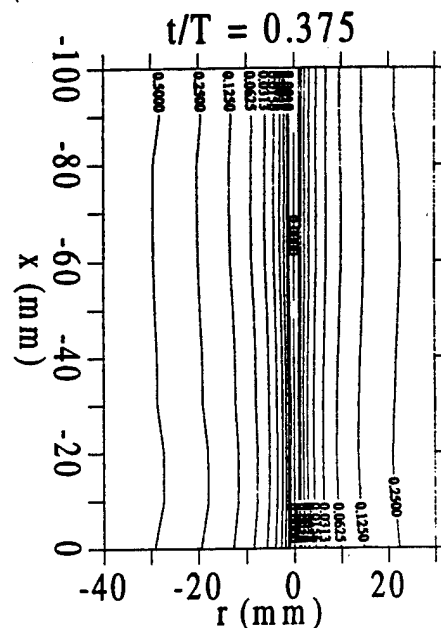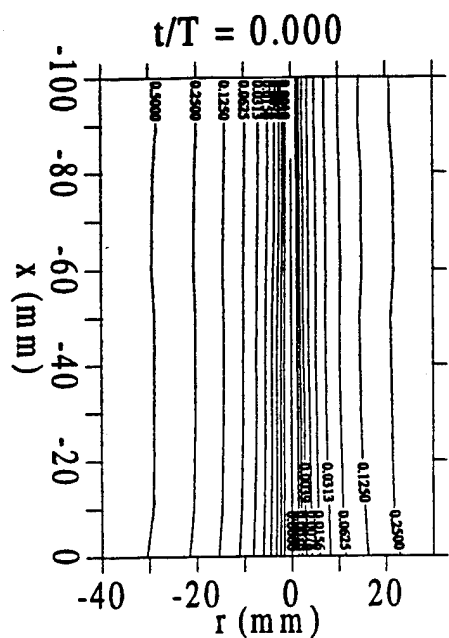
$$\frac{Q_m(X,r)}{Q_{max}} = \frac{2\pi \int_0^r \frac{V_x}{U_\infty} \eta d\eta}{2\pi \int_0^R \frac{V_x}{U_\infty} \eta d\eta}$$

Fig. 16 (a). Normalized mass-flow rate survey of a plane across the vortex core centerline during flow deceleration. $\alpha = 15$ deg, A = 1, k = 1.27, R = 0.42.
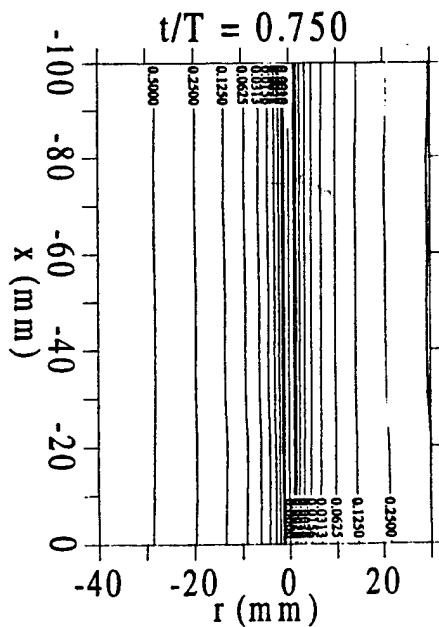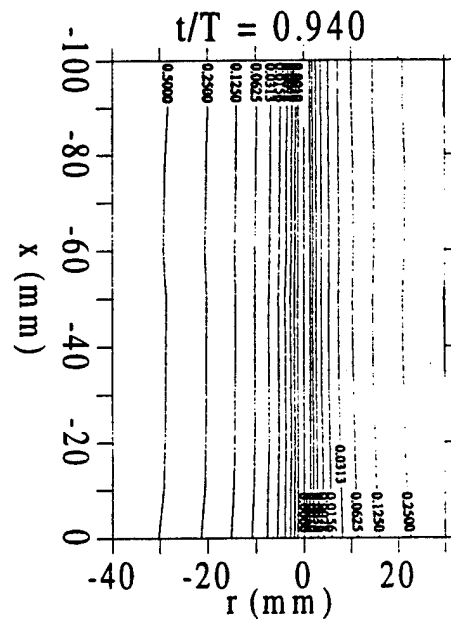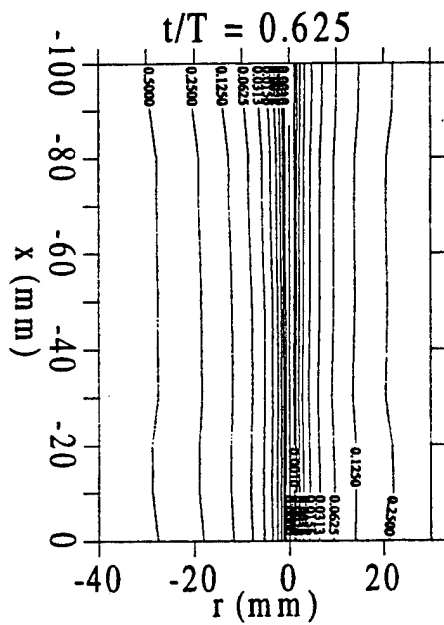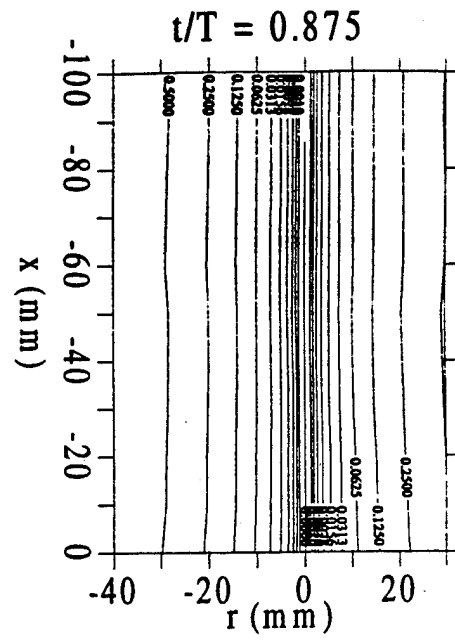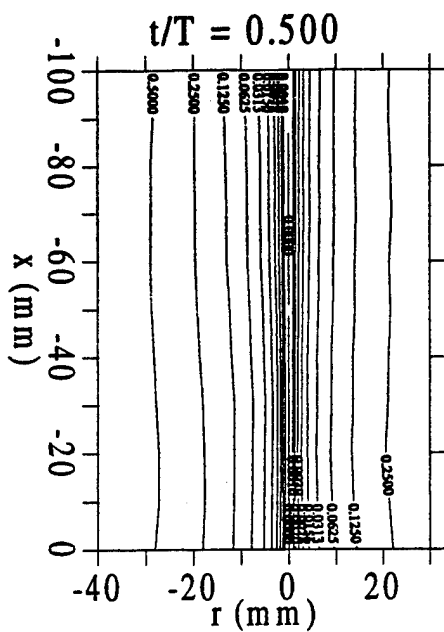
Fig. 16 (b). Normalized mass-flow rate survey of a plane across the vortex core centerline during flow acceleration. α = 15 deg, A = 1, k = 1.27, R = 0.42.

$$\frac{Q_m(X,r)}{Q_{max}} = \frac{2\pi \int_0^r \frac{V_x}{U_\infty} \eta d\eta}{2\pi \int_0^R \frac{V_x}{U_\infty} \eta d\eta}$$
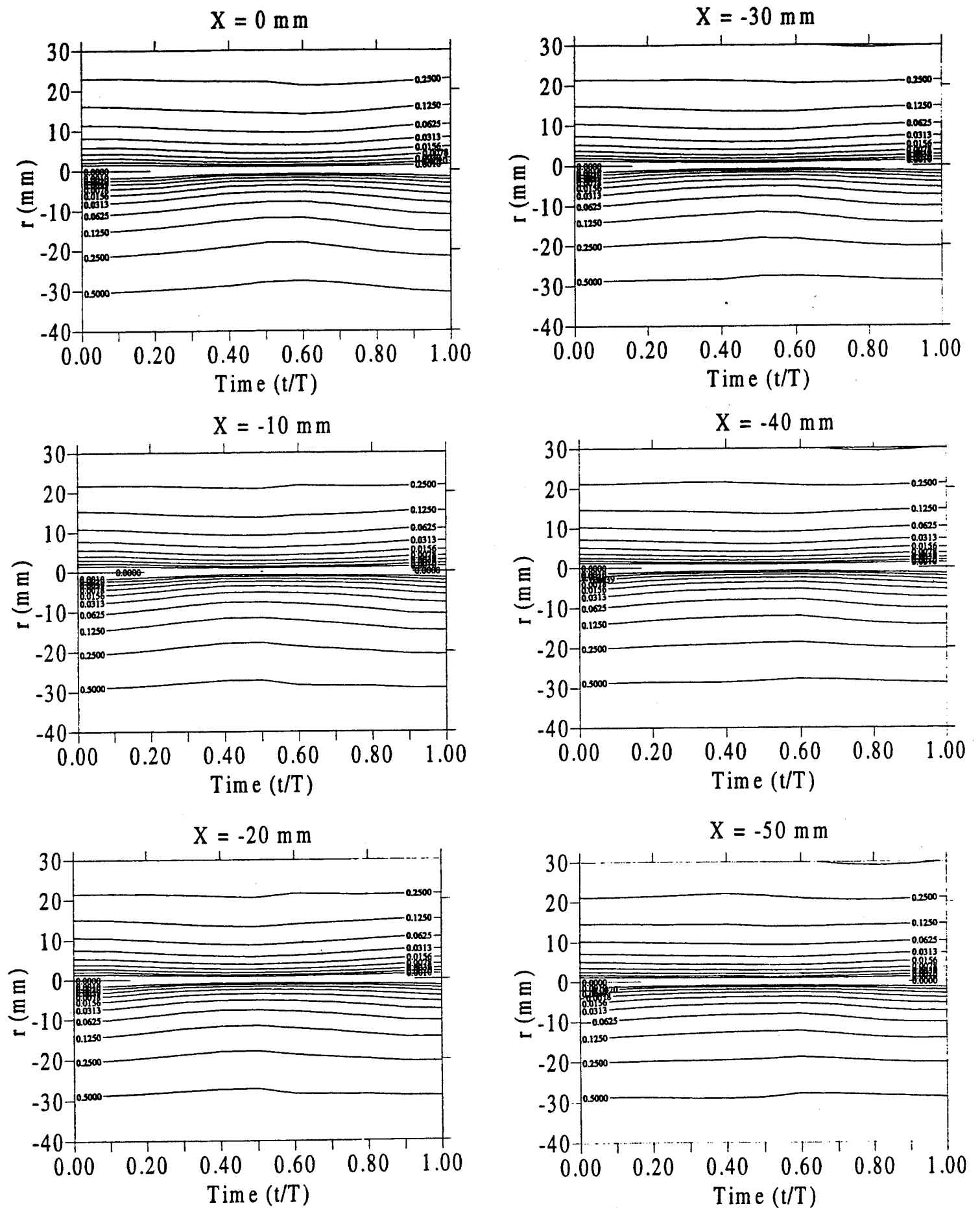
Fig. 17. Temporal variation of flowrate across the vortex core centerline at different axial locations. $\alpha = 15$ deg, $A = 1$, $k = 1.27$, $R = 0.42$.
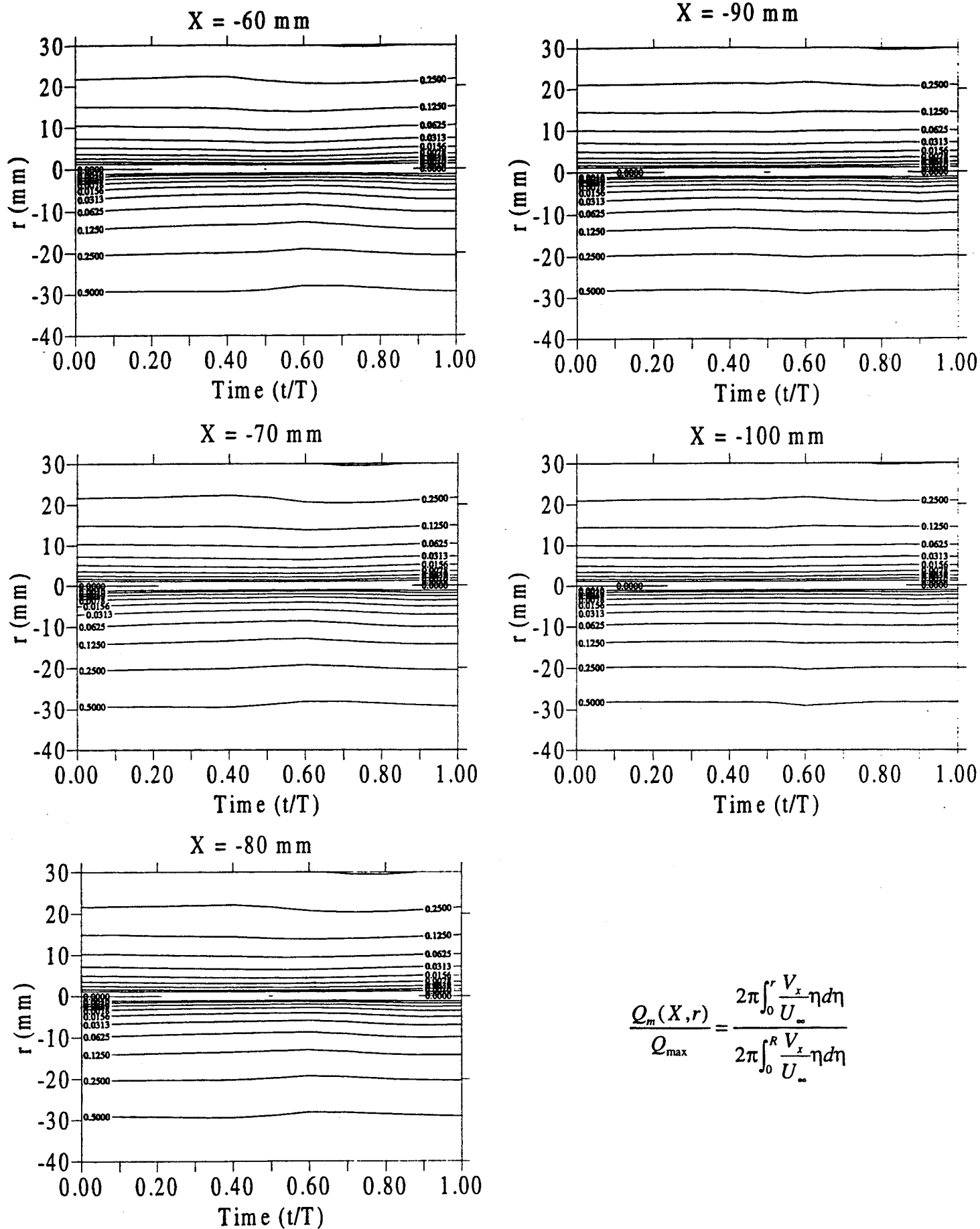
$$\frac{Q_m(X,r)}{Q_{max}} = \frac{2\pi \int_0^r \frac{V_x}{U_\infty} \eta \, d\eta}{2\pi \int_0^R \frac{V_x}{U_\infty} \eta \, d\eta}$$
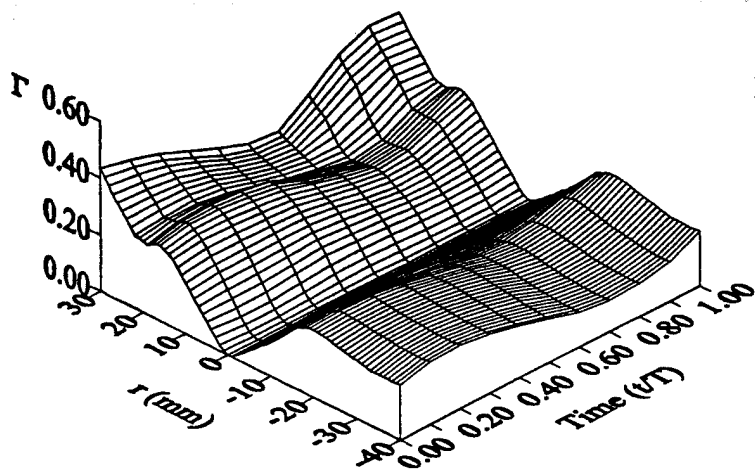
Fig. 17, Con't. Temporal variation of flowrate across the vortex core centerline at different axial locations. $\alpha = 15$ deg, A = 1, k = 1.27, R = 0.42.
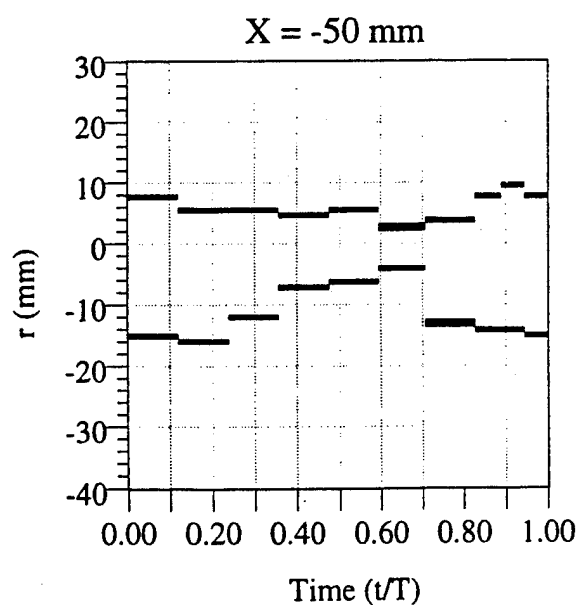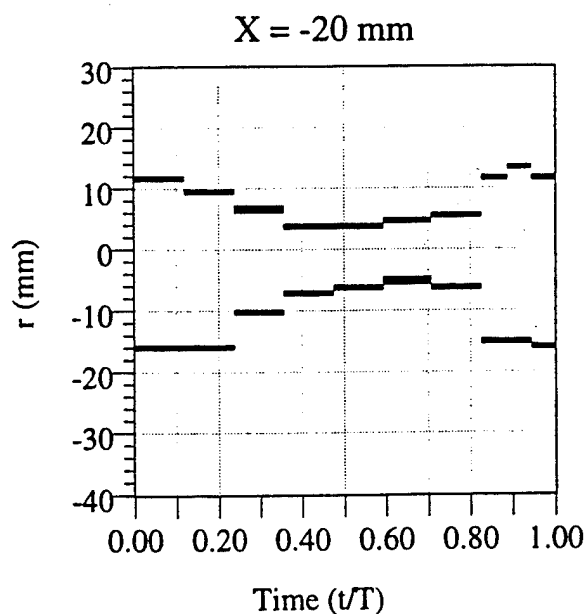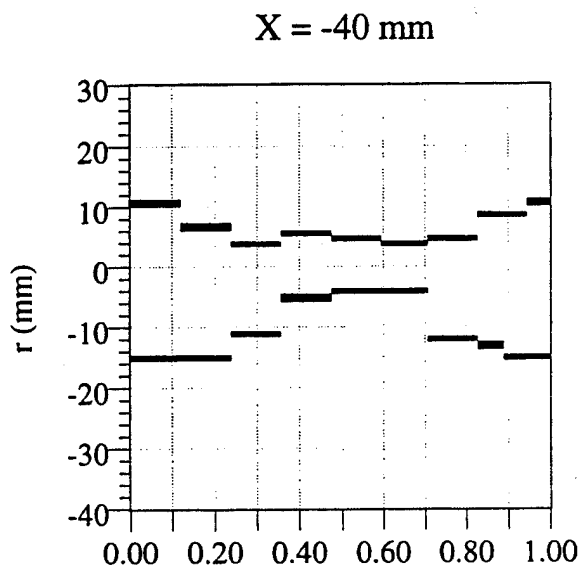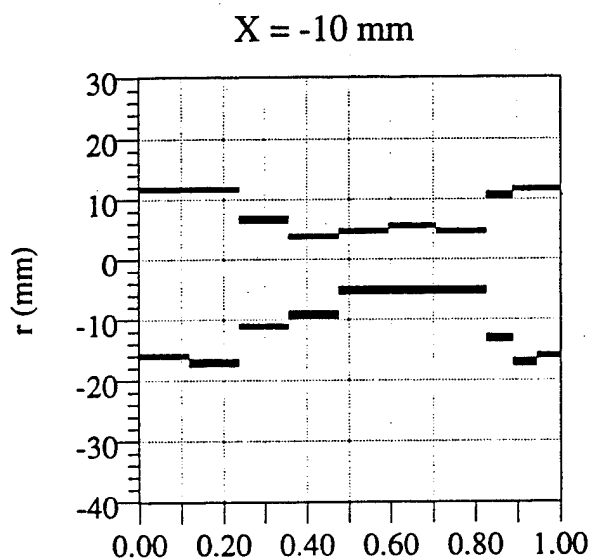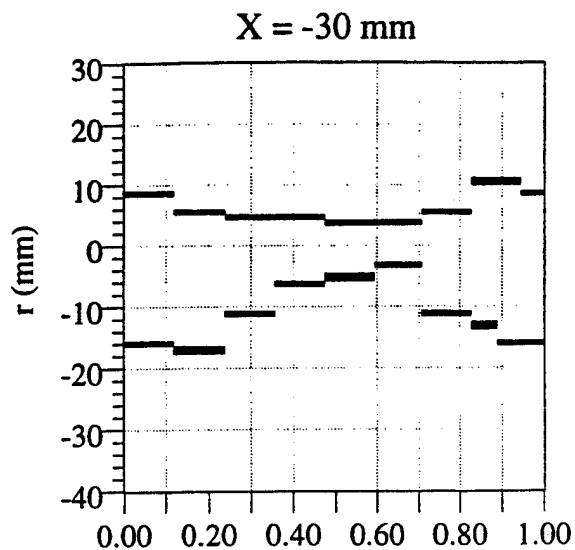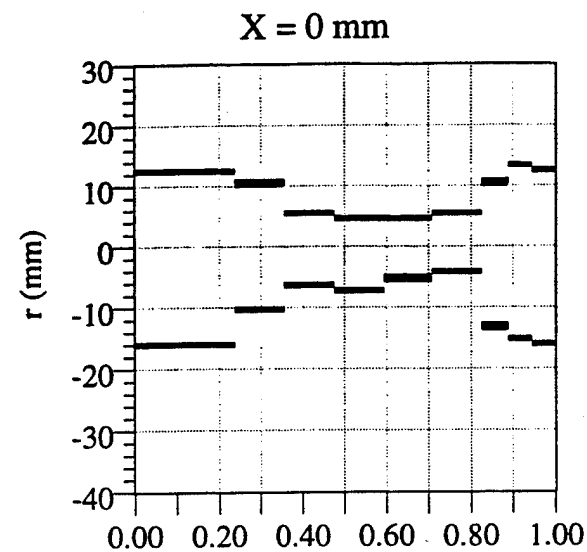
Fig. 18 (a). Temporal variation of vortex viscous core (r_c) size at different axial locations. α=15 deg, A = 1, k = 1.27, R = 0.42
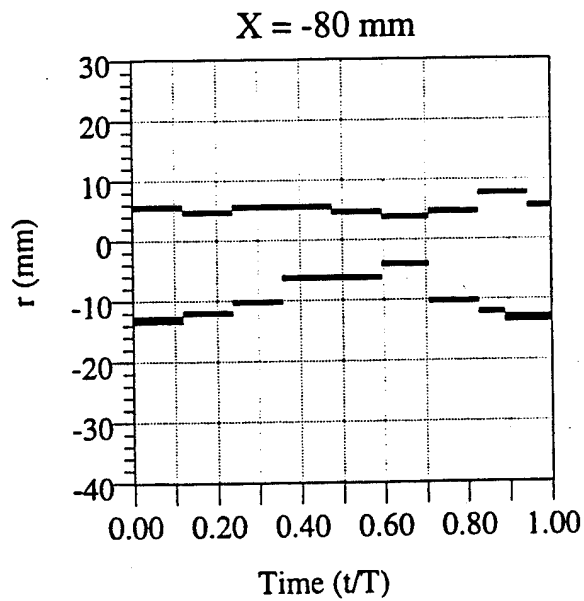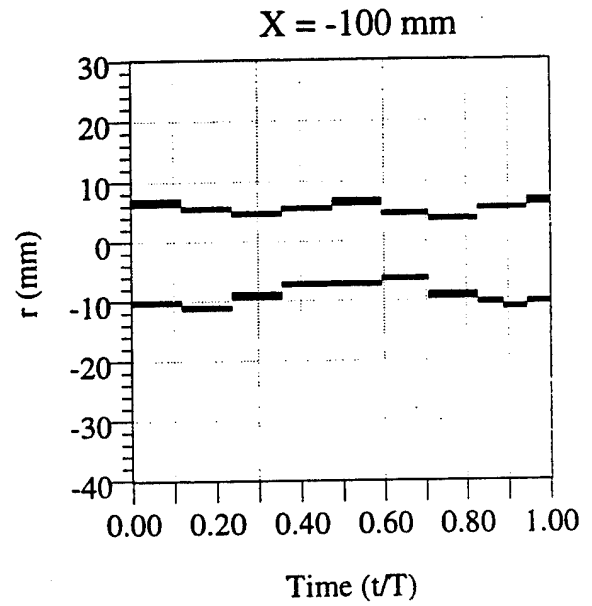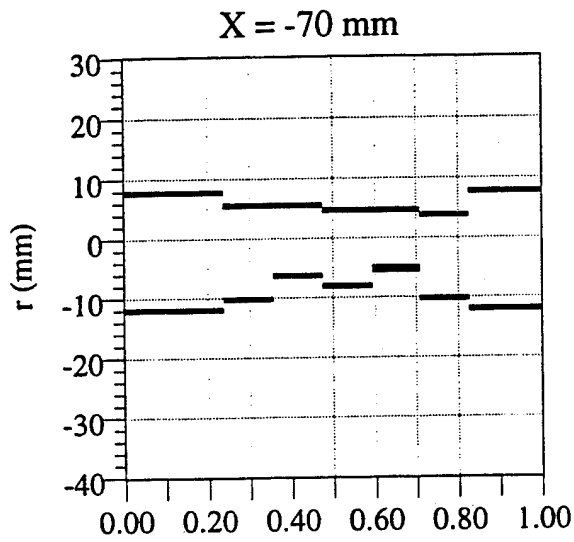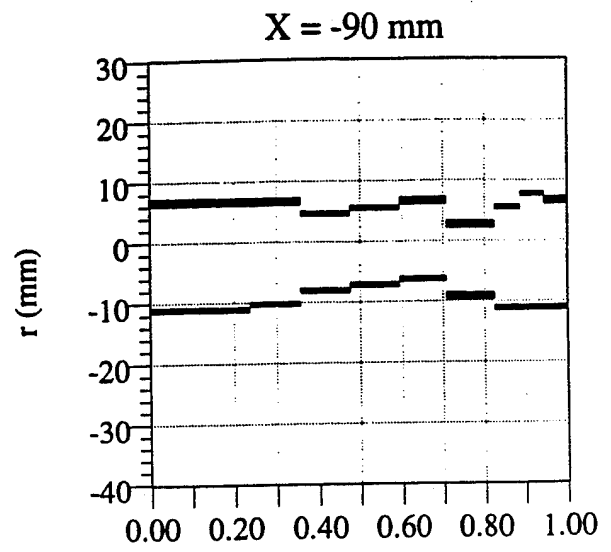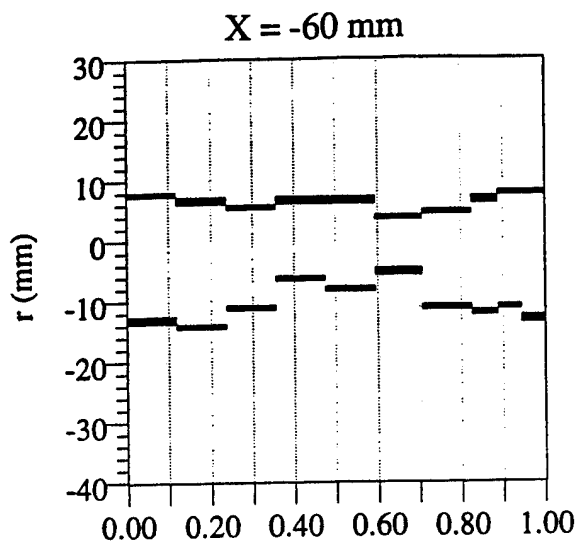
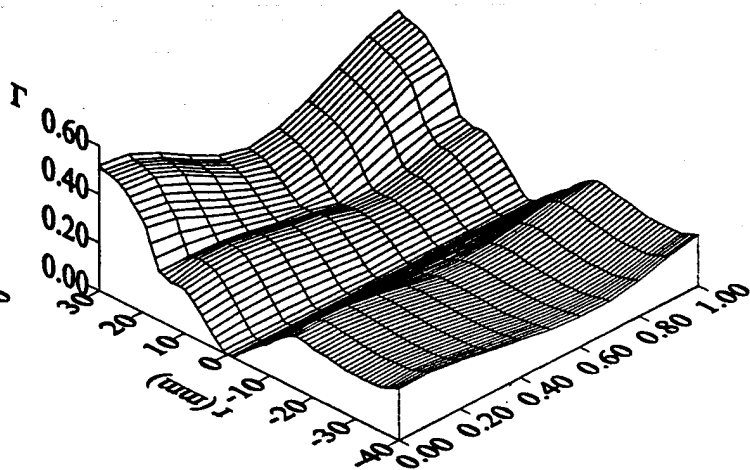Fig. 18 (b). Temporal variation of vortex viscous core (r_c) size at different axial locations. $\alpha=15$ deg, A = 1, k = 1.27, R = 0.42
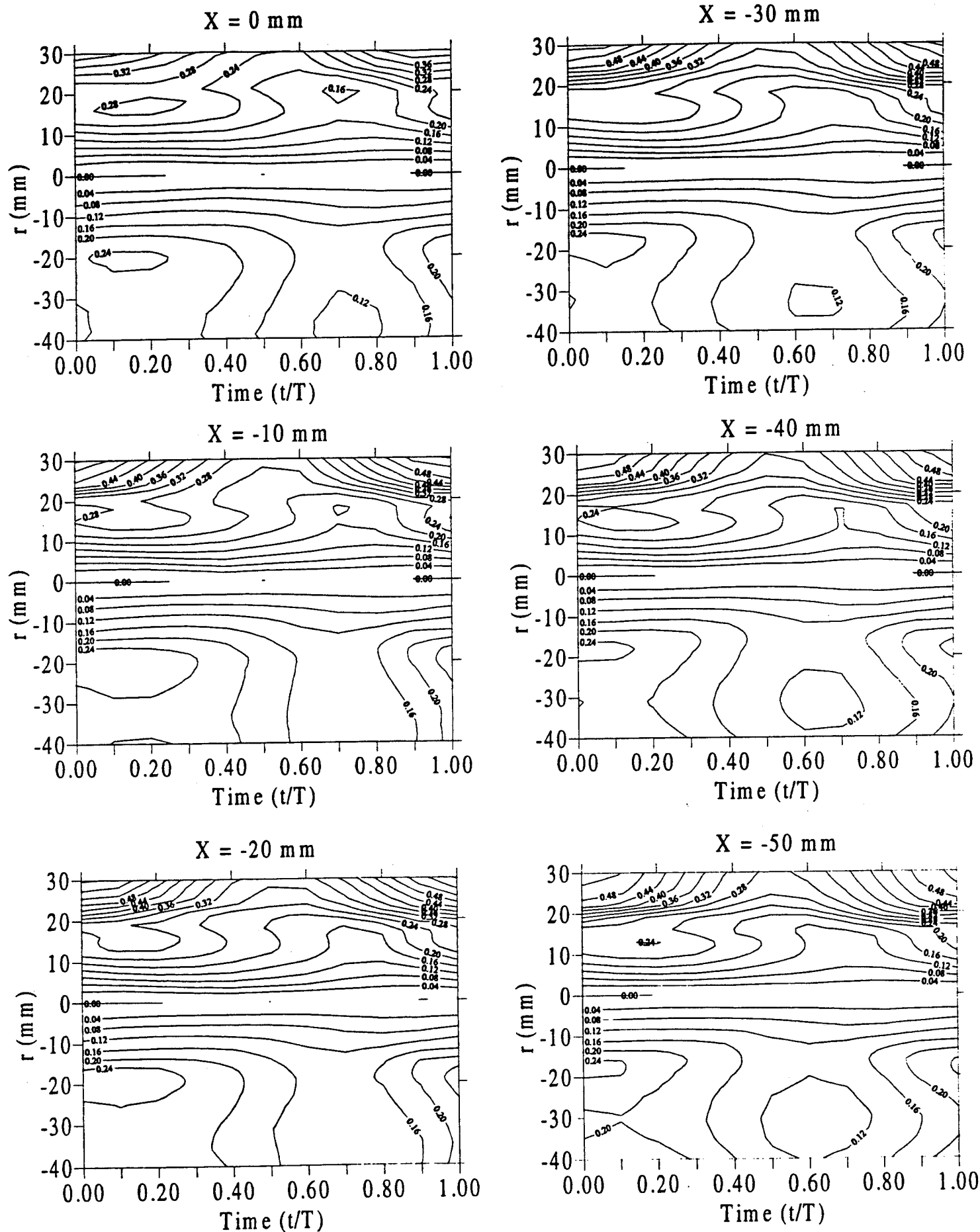
Fig. 19. Temporal variation of normalized circulation across the vortex core centerline at different axial locations. $\alpha = 15$ deg, $A = 1$, $k = 1.27$, $R = 0.42$.
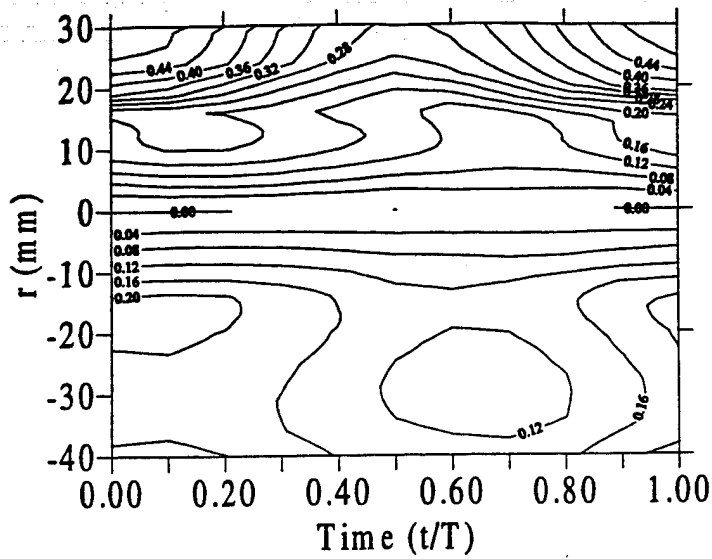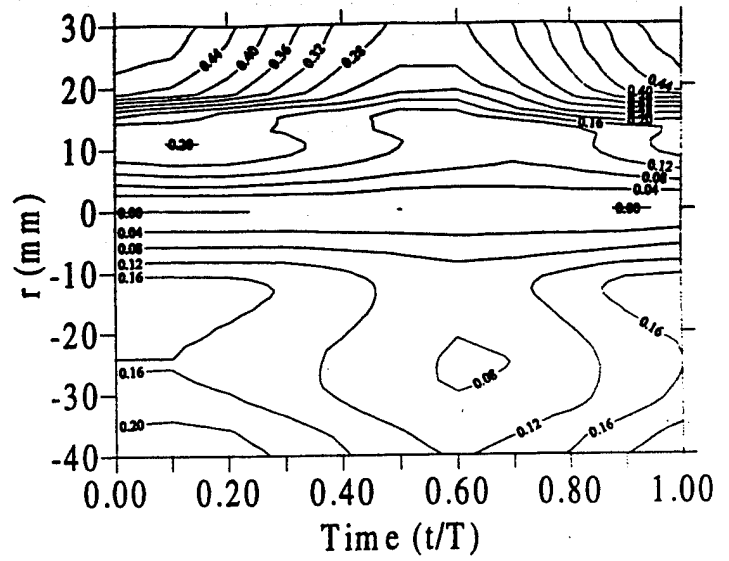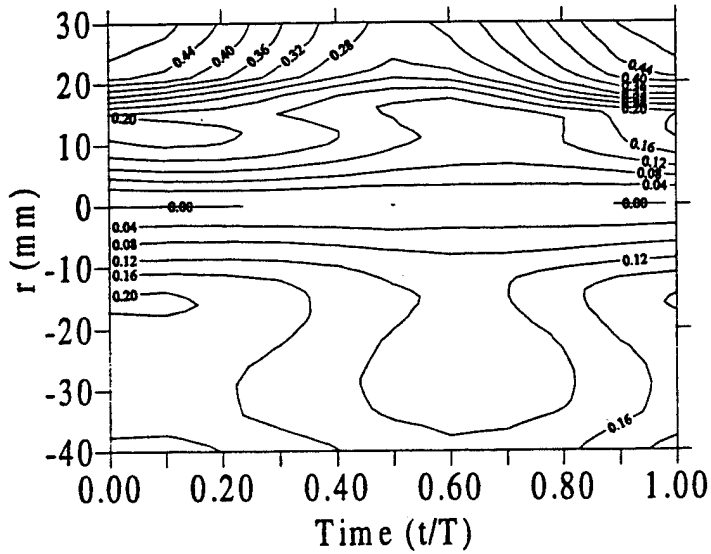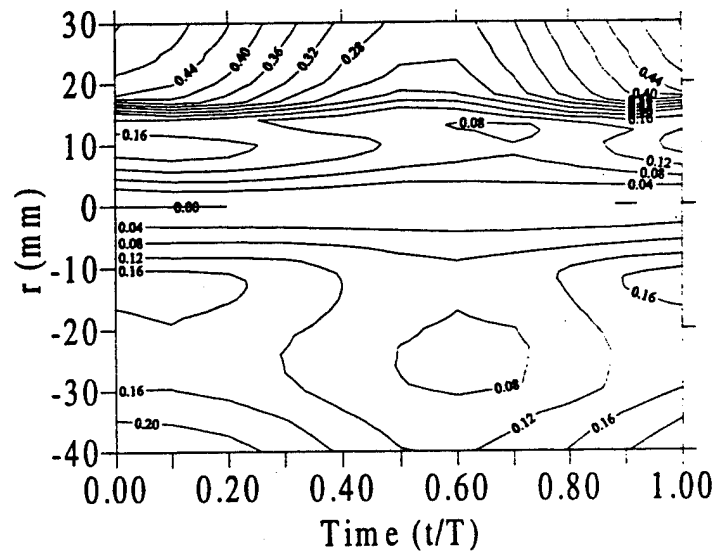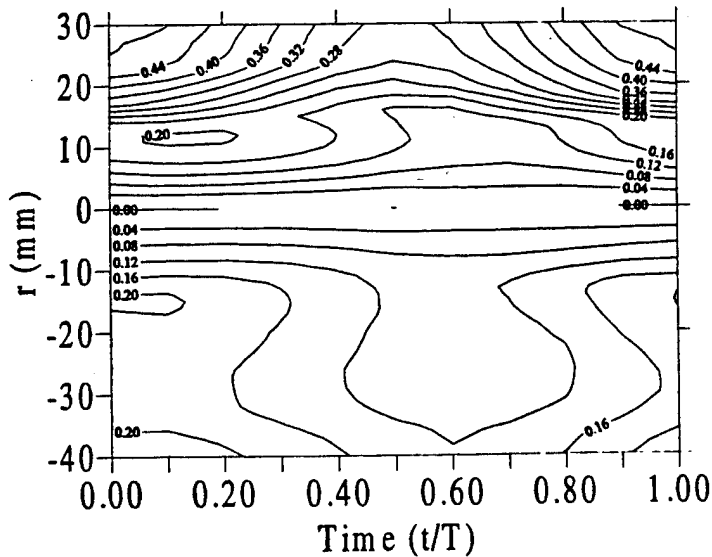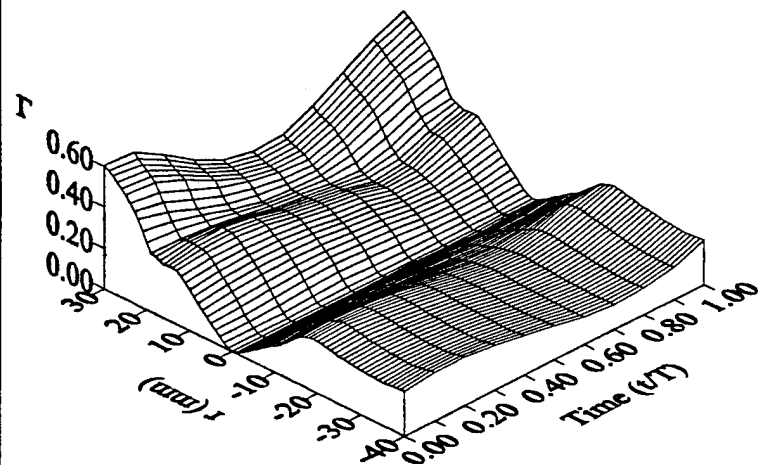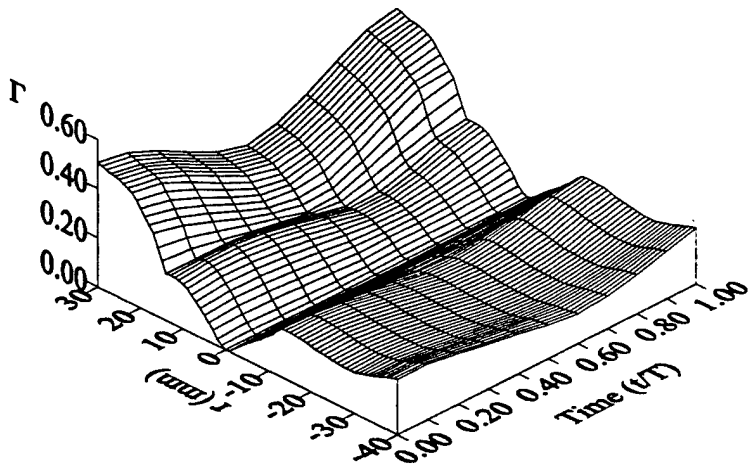
Fig. 19, Con't. Temporal variation of normalized circulation across the vortex core centerline at different axial locations. $\alpha = 15$ deg, A = 1, k = 1.27, R = 0.42.
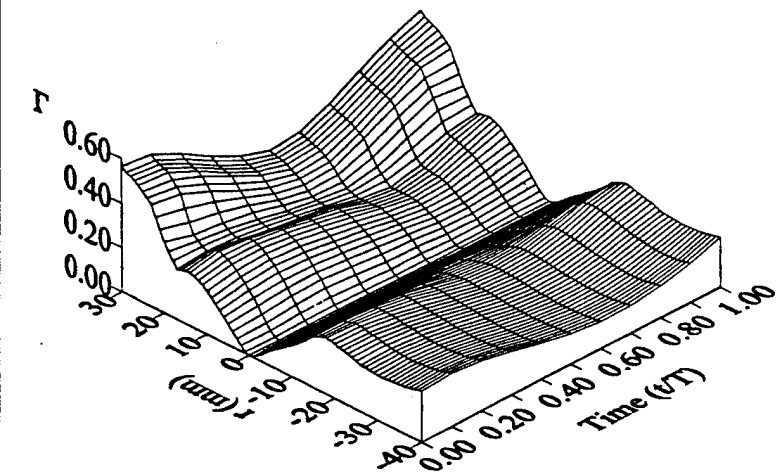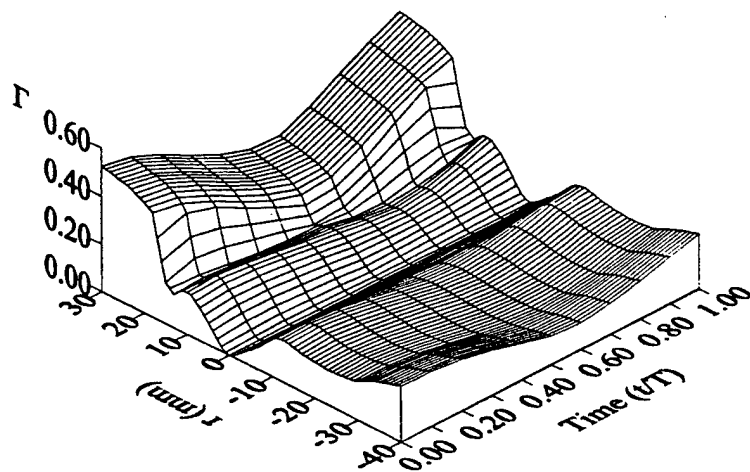
Fig. 20. Surface plot of the temporal variation of normalized circulation across the vortex core centerline at different axial locations. α=15 deg., A = 1, k=1.27, R = 0.42.